Received June 2, 2020, accepted June 18, 2020, date of publication June 22, 2020, date of current version July 1, 2020.

Digital Object Identifier 10.1109/ACCESS.2020.3004299

Multi-Verse Optimizer for Model Predictive Load Frequency Control of Hybrid Multi-Interconnected Plants Comprising Renewable Energy

HOSSAM HASSAN ALI[1], AHMED M. KASSEM[2], MUJAHED AL-DHAIFALLAH[3], (Member, IEEE), AND AHMED FATHY[4,5]

[1]Electrical Department, Faculty of Industrial Education, Sohag University, Sohag 82524, Egypt
[2]Electrical Engineering Department, Faculty of Engineering, Sohag University, Sohag 82524, Egypt
[3]Systems Engineering Department, King Fahd University of Petroleum and Minerals, Dhahran 31261, Saudi Arabia
[4]Electrical Engineering Department, Faculty of Engineering, Jouf University, Sakaka 72388, Saudi Arabia
[5]Electrical Power and Machine Department, Faculty of Engineering, Zagazig University, Zagazig 44516, Egypt

Corresponding authors: Mujahed Al-Dhaifallah (mujahed@kfupm.edu.sa) and Ahmed Fathy (afali@zu.edu.eg)

ABSTRACT This paper presents a recent metaheuristic optimization approach of multi-verse optimizer (MVO) to design load frequency control (LFC) based model predictive control (MPC) incorporated in large multi-interconnected system. The constructed system comprises six plants with renewable energy sources (RESs). MVO is employed to determine the optimal parameters of MPC-LFC to achieve the desired output of the interconnected system in case of load disturbances. The presented system comprises reheat thermal, hydro, photovoltaic (PV) model with maximum power point tracker (MPPT), wind turbine (WT), diesel generation (DG), and superconducting magnetic energy storage (SMES). The integral time absolute error (ITAE) of the frequencies and tie-line powers deviations is proposed as objective function. The effects of governor dead zone and generation rate constraint (GRC) of thermal plants are considered. The performance of the proposed MPC optimized via MVO is compared with the other designed via intelligent water drops (IWD) and genetic algorithm (GA). Additionally, the robustness of the proposed MPC-LFC based MVO with variation of the system parameters is presented. The obtained results confirmed the superiority and reliability of the proposed controller compared to the others.

INDEX TERMS Multi-verse optimizer, load frequency control, model predictive control.

I. INTRODUCTION

One of the most important issues in the power system operation is the stability of frequency, especially in case of disturbances. The desired frequency is achieved via incorporating load frequency control (LFC) in the system, it forces the deviations of the frequency and tie-line power to stabilize at zero. Power plants can be interconnected to share the loads and cover the generation deficiency at any station. This helps in keeping the system reliability in the event of failure of generation in one area [1], [2]. Recently, renewable energy sources (RESs) such as photovoltaic (PV) and wind turbine (WT) are integrated with traditional energy sources in multi-interconnected system [3]. Many reported studies were performed on designing LFC incorporated in the multi-interconnected system. A fractional order (FO) Fuzzy- proportional-integral-derivative (F-PID) controller based LFC has been optimized via bacterial foraging optimization (BFO). The presented LFC has been incorporated in a hydro-thermal system with redox flow batteries (RFB) [4]. Dash *et al.* [5] presented an optimized LFC based on cascaded proportional integral (PI) and proportional derivative (PD) controllers in nonlinear interconnected system via flower pollination algorithm (FPA). F-PID based LFC has been presented with three membership functions and tuned via improved grey wolf optimization (IGWO), hybrid harmony search cuckoo optimization algorithm (HSCOA) with high voltage direct current (HVDC) [6], [7]. Shahalami *et al.* [8]

The associate editor coordinating the review of this manuscript and approving it for publication was Shiwei Xia.

investigated the performance of LFC with HVDC link via a linear quadratic regulator (LQR) controller and Kalman filter. *Arya* [1] presented an imperialist competition algorithm (ICA) to optimize F-PID based LFC incorporated in two-interconnected system with PV and capacitive energy storage (CES). LFC based PID controller has been tuned via hybrid pattern search (PS) and gravitational search algorithm (GSA) [9]. *Babu et al.* [10] presented LFC optimized via crow search algorithm (CSA). It has been used for solar thermal and HVDC to minimize the performance index. PID based LFC has been designed via modified whale optimization algorithm (MWOA) employed in two-interconnected system comprising PV and thermal plants [11]. *Sharma et al.* [12] implemented six-interconnected area with hybrid LFC via interline power flow controller (IPFC) optimized by multi-verse optimizer (MVO). In Ref. [13], sin-cosine algorithm (SCA) has been employed to optimize the cascaded controller incorporated with the deregulated system of a dish-stirling solar thermal system (DSTS). Biogeography based optimized (BBO) has been introduced to optimize PID-LFC used in DSTS [14]. *Arya*. [15] presented Fuzzy-PID controller optimized via ICA in different interconnected systems. In Ref. [16], PID, and Sugeno Fuzzy logic (SFL) based LFC have been optimized via quasi-oppositional harmony search algorithm (QOHSA) and incorporated in deregulated system with thyristor-controlled series compensator (TCSC). In Ref. [17], Antlion optimizer (ALO) has been employed to simulate Fuzzy pre-compensated intelligent PID controller incorporated in a multi-interconnected system. *Sarkar et al.* [18] investigated robust adaptive sliding mode control (SMC) on three-interconnected plants. In Ref. [19], Fuzzy-PID with derivative filter based LFC has been optimized via COA in multi-source with HVDC. In Ref. [20], solar thermal plant including LFC has been presented with PID optimized via grey wolf optimizer (GWO). Lightning search algorithm (LSA) has been used in Ref. [21] to compute the optimal gains of the Integral-double derivative controller with derivative filter representing LFC with multi-source system. Ref. [22] studied Fuzzy-PID with fractional order based LFC incorporated in multi-interconnected system and optimized via BBO. Ref. [23] presented multi-source system with HVDC controlled via PID based LFC designed via invasive weed optimization (IWO), the performance index based on integral time absolute error (ITAE) is selected as the target. *Nosratabadi et al.* [24] studied the predictive modified PID based LFC optimized via the grasshopper optimization algorithm (GOA). *Raju et al.* [25] presented PI with fractional derivative (PIDμ) controller optimized via hybrid antlion optimizer (ALO) based PS for LFC with distributed generation and flexible AC transmission system (FACTS). *Dhundhara et al.* [26] improved the performance of the deregulated system through CES and thyristor-controlled phase shifter (TCPS) with tie-line. A modified integral derivative (MID) optimized via hybrid differential evolution (DE) and PS has been presented in Ref. [27] for two-interconnected system. Reference [28] presented PID based LFC designed via linear matrix inequality (LMI) incorporated in single and two-interconnected systems. In Ref. [29], gases brownian motion optimization (GBMO) has been employed to optimize Fuzzy-PID based LFC. Elsisi *et al.* [30], [31] presented model predictive control (MPC) based LFC optimized via bat-inspired algorithm (BIA) employed in hydro-thermal interconnected system. In Ref. [32], salp swarm algorithm (SSA) has been employed to optimize PID-LFC incorporated in multi-interconnected system with WT and PV arrays. Additionally, the effects of real wind speed and solar radiation intensity have been studied. PID based LFC optimized via improved stochastic fractal search algorithm (ISFS) has been presented in [33] considering ITAE as the target. Electro search optimizer (ESO) modified by balloon effect has been employed to design an adaptive integral based LFC controller [34]. Fuzzy-PID based LFC incorporated in multi-interconnected system and optimized via the modified sine cosine algorithm (MSCA) has been presented in [35]. Reference [36] studied the deregulated LFC based tilted integral derivative (TID) controller optimized via hybrid teaching-learning based optimization and pattern search (hTLBO-PS) approach. The MPC based LFC has been presented with economic costs and very short-term load forecasting (VSTLF) to minimize the frequency fluctuation in single area [37]. A generalized multi-period economic dispatch (GMPED) problem has been studied with MPC based LFC integrated renewable energy and controllable load via bi-level optimization [38]. A system comprising renewable energy, grid-friendly appliances (GFAs), and energy storage units incorporated in LFC system based MPC has been introduced in [39].

Most of the reported methods did not touch the application of their approaches on large multi-interconnected system. Most of them dealt with simple interconnected system with ignoring some details of governor dead zone and generation rate constraint of thermal plants, and such models are far from reality. Additionally, few researchers presented multi-interconnected system, including RESs. Furthermore, methods used metaheuristic approaches required large number of controlling parameters which may cause falling in local optima. Therefore, all these defects are considered in our work to cover this gap.

The contribution of this work can be summarized as follows:

- A new approach based on multi-verse optimizer (MVO) is proposed to determine the optimal parameters of model protective control (MPC) based LFC incorporated in large multi-interconnected system with conventional and renewable energy plants.
- A new architecture of multi-interconnected system comprising PV, WT, hydro, thermal, and diesel generator-based plants is constructed and the proposed MPC based LFC is incorporated and investigated on the proposed architecture.

- Sensitivity analysis is implemented via changing some parameters of the constructed multi-interconnected system.
- The robustness of the proposed MPC-LFC optimized via MVO under variable wind power is confirmed.

The paper is outlined as: section II presents the mathematical model of the multi-interconnected system, section III introduces the main principle of the multi-verse optimizer, section IV explains the proposed optimization problem, section V introduces simulation results, and section VI presents conclusion.

II. MATHEMATICAL MODEL OF THE PROPOSED MULTI-INTERCONNECTED SYSTEM

The proposed system presented in this work comprises six plants of thermal, hydro, diesel generator (DG), PV with MPPT, and WT generation plants with SMES as storage system. The architecture of the proposed multi-interconnected system is shown in Fig. 1.

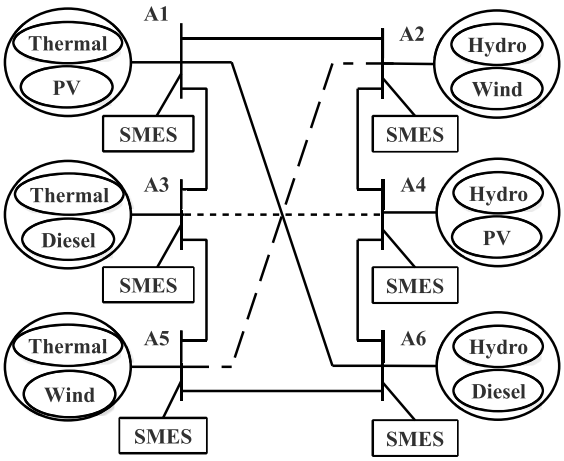

FIGURE 1. Architecture of the proposed multi-interconnected system.

A. THERMAL PLANT MODEL

The block diagram of the thermal generation unit is shown in Fig. 2, it can be described as follows [40]:

$$\text{Governor model } G_g = \frac{K_g}{T_g s + 1} \tag{1}$$

$$\text{Reheater model } G_r = \frac{K_r T_r s + 1}{T_r s + 1} \tag{2}$$

$$\text{Steam turbine model } G_t = \frac{K_t}{T_t s + 1} \tag{3}$$

$$\text{Generator model } G_{gen} = \frac{K_p}{T_p s + 1} \tag{4}$$

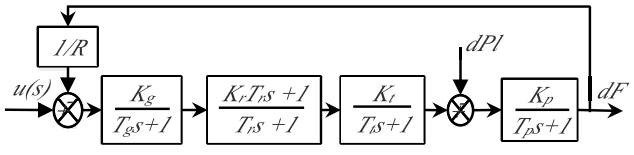

FIGURE 2. Block diagram of thermal generating unit.

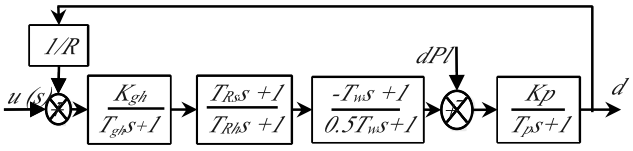

FIGURE 3. Block diagram of hydro generation unit.

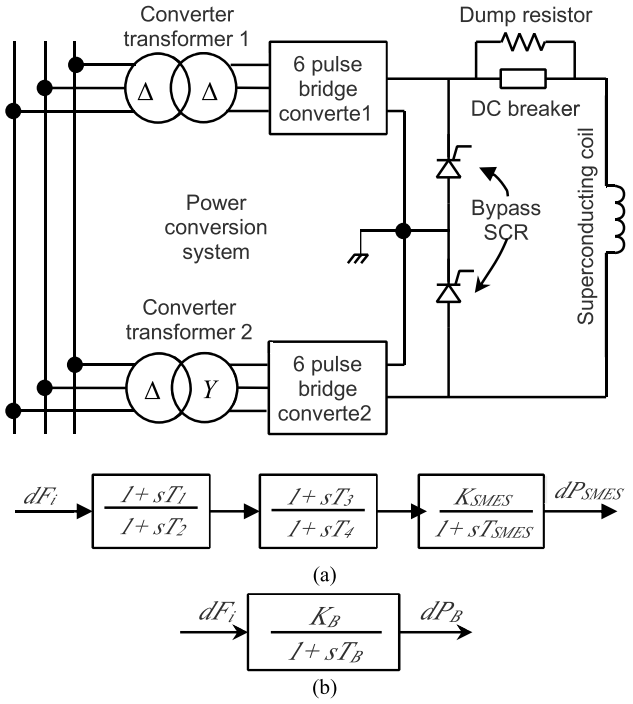

FIGURE 4. (a) Structure and block diagram of SMES. (b) Block diagram of battery.

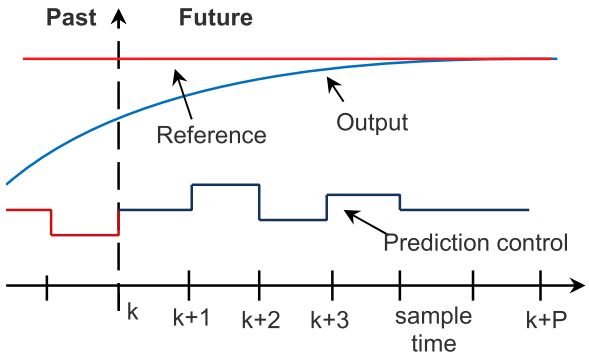

FIGURE 5. Theory of MPC.

where K_p, K_t, K_r, and K_g are generator, turbine, reheater, and governor gains while T_p, T_t, T_r, and T_g are generator, turbine, reheater and governor time constants.

B. HYDRO PLANT MODEL

The block diagram of the hydro generation unit is shown in Fig. 3. It can be described as follows [41]:

$$G_{MHG} = \frac{K_{gh}}{T_{gh} s + 1} \times \frac{T_{Rs} s + 1}{T_{Rh} s + 1} \tag{5}$$

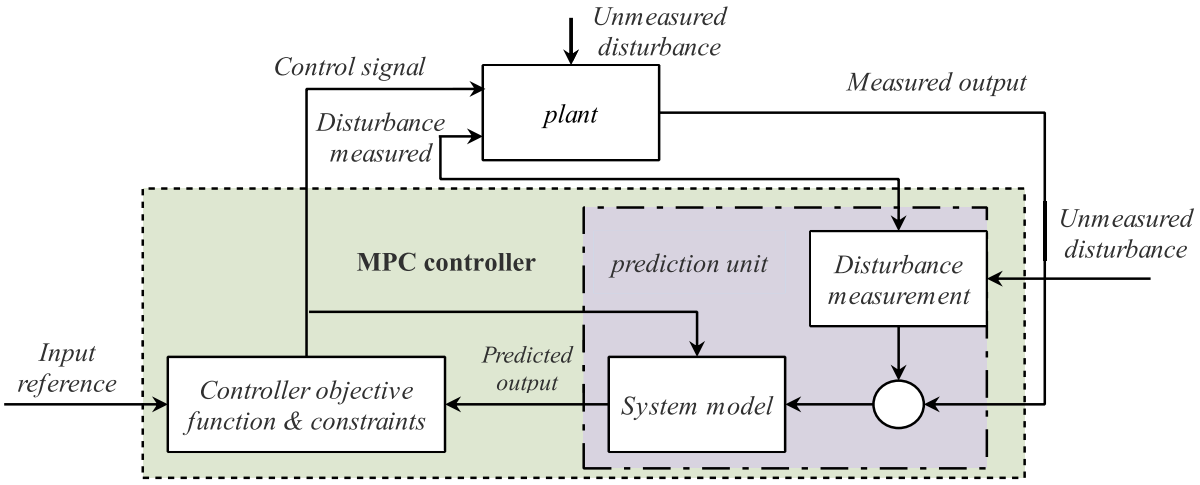

FIGURE 6. Structure of MPC.

$$G_t = \frac{-T_w s + 1}{0.5T_w s + 1} \tag{6}$$

where K_{gh} and T_{gh} are the gain and time constant of the governor, T_{Rs} and T_{Rh} are the transient droop and reset time constants of the hydro governor, and T_w is the nominal start time of the water in penstock.

C. PHOTOVOLTAIC PLANT MODEL

PV cells are usually connected in series and parallel to meet the demand. Due to the change of solar radiation throughout the day, the relation between voltage and current is nonlinear. It is essential to use maximum power point tracker (MPPT) for enhancing the output power of the PV panel. The transfer function of the PV plant with MPPT can be described as follows [1], [42]:

$$G_{PV} = \frac{K_{PV1}s + K_{PV2}}{s^2 + T_{PV1}s + T_{PV2}} \tag{7}$$

where K_{PV1} and K_{PV2} are the gains of the PV system with MPPT, T_{PV1} and T_{PV2} are the time constants of the PV system. The approach used in extracting the MPP from the PV system is incremental conductance (IC). The conditions followed in IC can be expressed as follows:

$$\begin{cases} \dfrac{dP_{PV}}{dV_{PV}} > 0 \text{ At right of MPP} \\ \dfrac{dP_{PV}}{dV_{PV}} = 0 \text{ At MPP} \\ \dfrac{dP_{PV}}{dV_{PV}} < 0 \text{ At left of MPP} \end{cases} \tag{8}$$

D. WIND GENERATION PLANT MODEL

In this study, doubly-fed induction generator (DFIG) based wind turbine (WT) is considered. The wind energy is converted into electricity via WT which is considered as prime mover. The output power of the WT can be described as follows [43]:

$$P_W = 0.5\rho A C_P V_W^3 \tag{9}$$

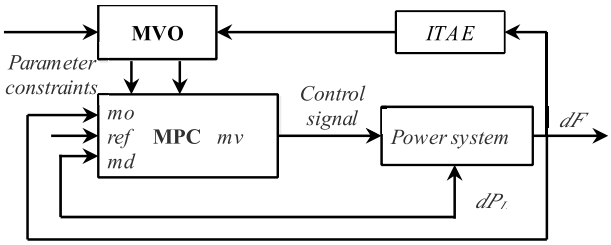

FIGURE 7. The proposed MPC optimized via MVO.

where ρ is the air density, A is the swept area of WT blades, C_p is the power coefficient, and V is the wind speed. The power coefficient of the WT can be written as follows:

$$C_p(\lambda, \beta) = (0.44 - 0.0167\beta)\sin\left(\frac{\pi(\lambda - 2)}{15 - 0.3\beta}\right) - 0.00184(\lambda - 3) \tag{10}$$

where λ is the tip speed ratio, and β is the blade pitch angle. The transfer function of the wind plant can be written as follows [27], [44]:

$$G_W = \frac{K_{pw1}(1 + sT_{pw1})}{1 + s} \times \frac{K_{pw2}}{1 + sT_{pw2}} \times \frac{K_{pw3}}{1 + s} \tag{11}$$

where K_{pw1}, K_{pw2}, and K_{pw3} are the gains of the wind plant and T_{pw1}, T_{pw2}, and T_{pw3} are the time constants of the wind plant system.

E. DIESEL GENERATOR MODEL

In hybrid power system, the diesel generator (DG) is considered as an extra unit that provides electrical power output via a synchronous generator that is connected to the diesel engine [45]. The transfer function of DG can be described as follows [46]:

$$G_D = \frac{K_{dies}(1 + s)}{0.025s^2 + s} \tag{12}$$

F. MODEL OF SMES

Energy storage units such as superconducting magnetic energy storage (SMES), batteries, and flywheel are installed

TABLE 1. Comparison between the errors obtained via the MVO, GA, AND IWD.

Algorithm	ITAE	IAE	ITSE	ISE
IWD with installed RESs	3.5389	0.2684	0.0030	0.0008
GA with installed RESs	3.3232	0.3121	0.0042	0.0011
MVO without installed RESs	3.2348	0.2871	0.0030	0.0066
MVO with installed RESs	2.0833	0.2089	0.0018	0.0007
MVO with installed RESs and SMES	0.3131	0.0776	0.0003	0.0002

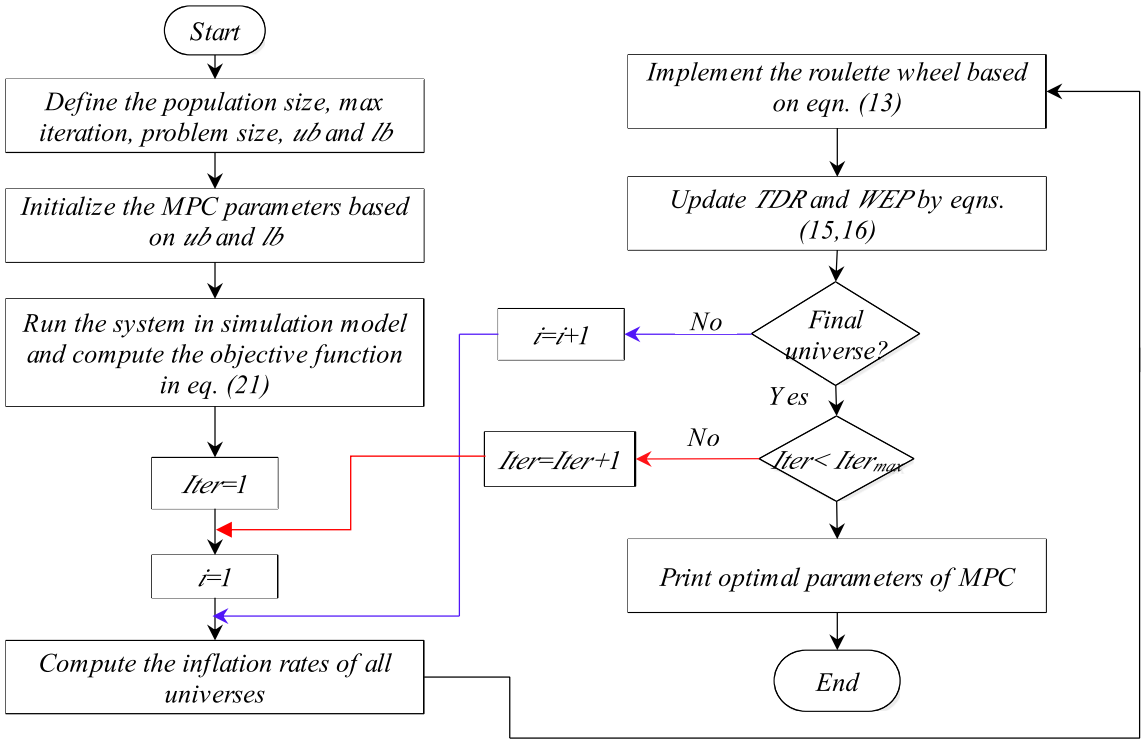

FIGURE 8. The proposed steps of the optimization approach.

in the power system to store the excess energy generated from the power plants. In this work, SMES is considered and its structure and block diagram are shown in Fig. 4. [47].

In case of fast response of the SMES, the delays caused by the frequency measurement can be modeled via the block diagram shown in Fig. 4(a). When the load demand is changed suddenly, the SMES discharges the stored energy into the grid via the power conversion system. SMES helps in enhancing the generated energy to minimize the time consumed by the system to be stable. While LFC operates to restore the current in the coil back to its primary value, the coil is charged by the surplus power in the system. The SMES is different than the battery in structure and transfer function as shown in Fig. 4. The SMES transfer function is based on two stage lead-lag compensator [47]–[50]. The SMES life is not affected by its ability to charge/discharge in a short time and ideally reduces the deviation in frequency. However, the battery life is affected by sudden charge/discharge currents. To compensate for power system disturbance before LFC operates, the energy storage system should have a fast-dynamic response. In addition, the charge/discharge speed of the battery is much slower than that of the SMES, Therefore, SMES is selected [51].

G. MAIN PRINCIPLE OF MULTI-VERSE OPTIMIZER

Multi-verse optimizer (MVO) was introduced by *Mirjalili* in 2016 [52], the MVO theory is based on astrophysics. The multi-verse describes how big bangs create countless universes and how they interact with each other through different types of holes such as worm, black, and white. Physicists stated that, more than one major explosion generates the birth of universe. Multi-verses approach runs counter to universe, despite a tunnel that represents the motion between two universe pairs and the interacts between white and black. White holes emit all while black holes attract all. The purpose of the white holes in MVO is to be at high universe inflation rates, while and black holes are assumed to have tiny inflation rate universes. Thus, events are migrated from the elevated

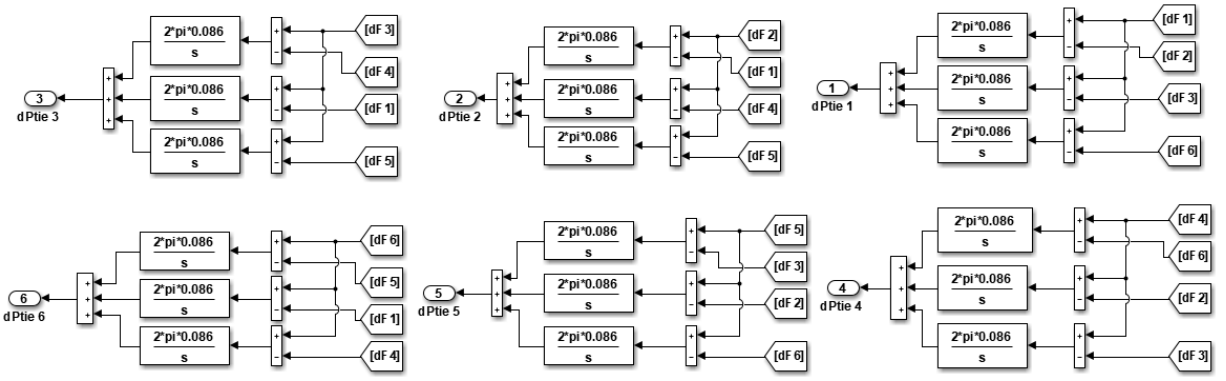

(a)

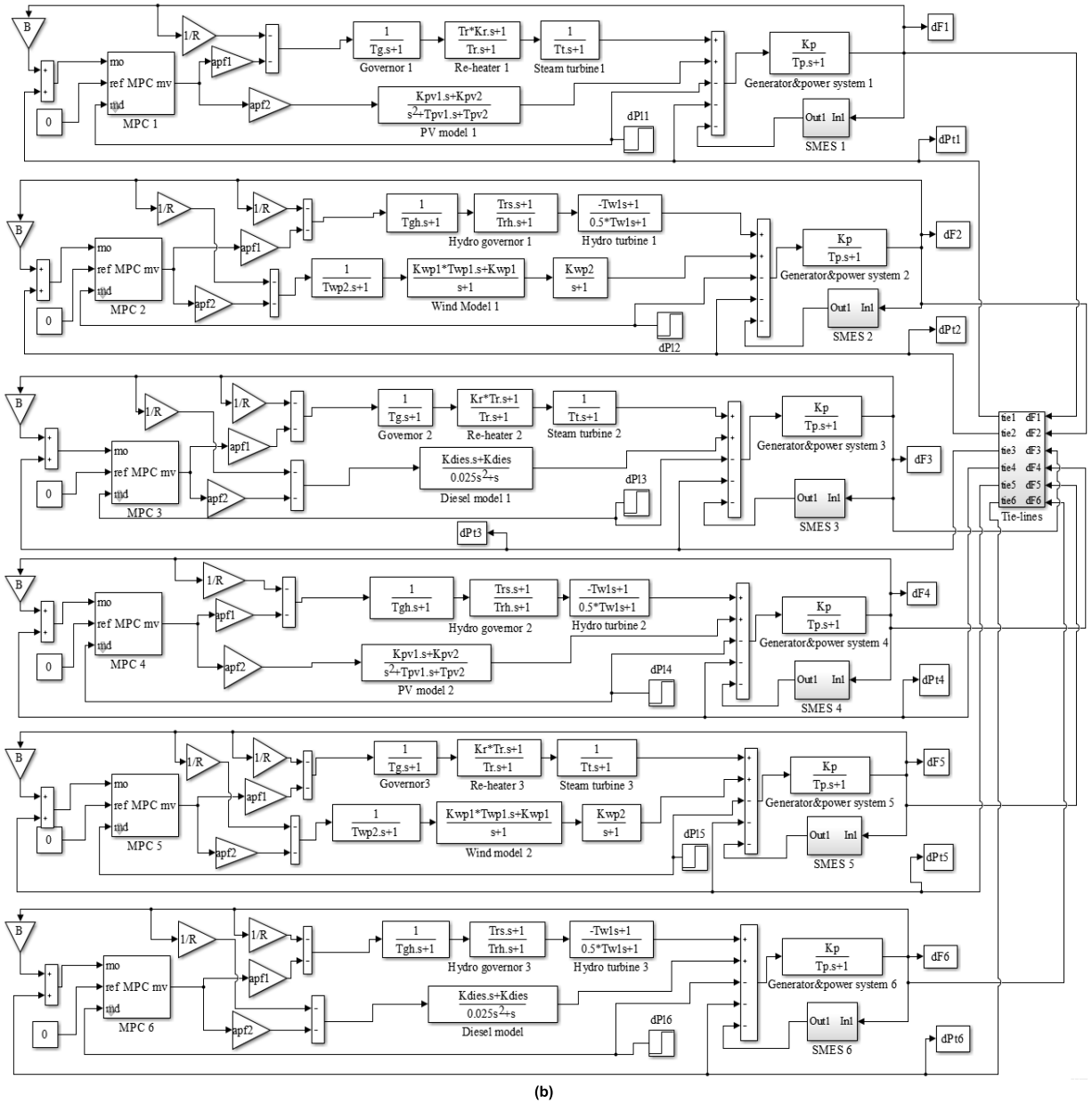

(b)

FIGURE 9. (a) Connection of tie-lines between plants. (b) Simulink model of six-interconnected system.

TABLE 2. Optimal parameters of MPC-LFC obtained via various approaches.

Algorithm	Controller number	Parameter				
		T	P	M	R	Q
IWD with installed RESs	MPC1	2.7336	8.0000	4.0000	8.1901	7.7306
	MPC2	9.1401	9.0000	4.0000	7.5563	3.7070
	MPC3	2.4442	9.0000	4.0000	7.3883	9.2428
	MPC4	6.7927	8.0000	4.0000	8.4024	7.0810
	MPC5	3.0782	6.0000	4.0000	2.5375	6.6518
	MPC6	2.9719	10.000	4.0000	7.0155	6.7707
GA with installed RESs	MPC1	1.3100	9.0000	3.0000	9.5070	2.244
	MPC2	0.5760	7.0000	1.0000	3.6410	4.9320
	MPC3	0.4310	8.0000	4.0000	9.3940	6.6360
	MPC4	1.7570	9.0000	2.0000	3.1380	9.6550
	MPC5	2.9210	7.0000	4.0000	5.9190	6.9260
	MPC6	1.3420	6.0000	4.0000	8.0970	3.5370
MVO Without installed RESs	MPC1	2.3224	5.000	4.0000	1.0108	8.7450
	MPC2	7.2258	4.0000	2.0000	9.9884	1.0271
	MPC3	6.4709	4.0000	2.0000	9.2641	1.0084
	MPC4	7.3606	8.0000	1.0000	7.0030	5.4109
	MPC5	9.0723	5.0000	3.0000	8.7496	1.4363
	MPC6	0.1571	8.0000	2.0000	1.5220	6.5487
MVO with installed RESs	MPC1	2.2143	9.0000	2.0000	3.8793	6.8896
	MPC2	2.0188	8.0000	2.0000	10.0000	9.5364
	MPC3	0.1075	5.0000	3.0000	3.8781	9.9603
	MPC4	1.3673	5.0000	1.0000	5.6063	1.4530
	MPC5	9.0235	6.0000	3.0000	9.0555	3.5808
	MPC6	6.5328	5.0000	1.0000	8.0829	4.8242
MVO with installed RESs and SMES	MPC1	1.3927	8.0000	4.0000	6.2463	4.3359
	MPC2	6.4463	10.000	2.0000	9.8065	5.9359
	MPC3	0.1150	5.0000	2.0000	6.2486	9.6452
	MPC4	1.6926	5.0000	2.0000	5.6864	6.0077
	MPC5	3.6014	8.0000	1.0000	8.4768	6.6608
	MPC6	7.8793	6.0000	1.0000	9.7059	1.1010

inflation globe to the reality that low inflation is through the white/black hole tunnels. This action guarantees the enhancement of the inflation rate of the entire universes. Modeling this action is performed based on the roulette wheel scheme. The universes were structured in each iteration according to the space of inflation that is accountable for the development of the universe. After that, only one universe is selected with white holes through the roulette wheel as follows:

$$X_i^j = \begin{cases} X_k^j, & r_1 < \mathrm{U}_i \\ X_i^j, & r_1 \geq \mathrm{U}_i \end{cases} \tag{13}$$

where X_i^j refers to the j^{th} coefficient of i^{th} universe, $X_k{}^j$ is the j^{th} coefficient of the k^{th} universe, r_1 is a random number in the range of [0,1], and U_i is the i^{th} universe normalized inflation rate. The updating process followed in MVO can be written as (14), shown at the bottom of the page, where X_j is the j^{th} parameter of the greatest universe, ub and lb are the upper and lower bounds respectively, and r_2, r_3, and

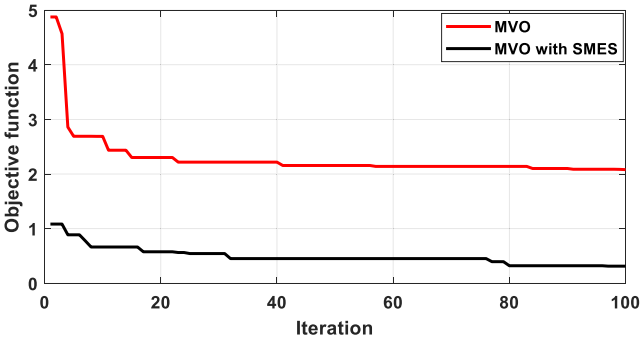

FIGURE 10. Performance of the objective function with iteration.

$$X_i^j = \begin{cases} \begin{cases} X_j + TDR \times ((ub - lb) \times r_4 + lb), & r_3 < 0.5 \\ X_j - TDR \times ((ub - lb) \times r_4 + lb), & r_3 \geq 0.5, \end{cases} & If\ r_2 < WEP \\ X_i^j, & If\ r_2 \geq WEP \end{cases} \tag{14}$$

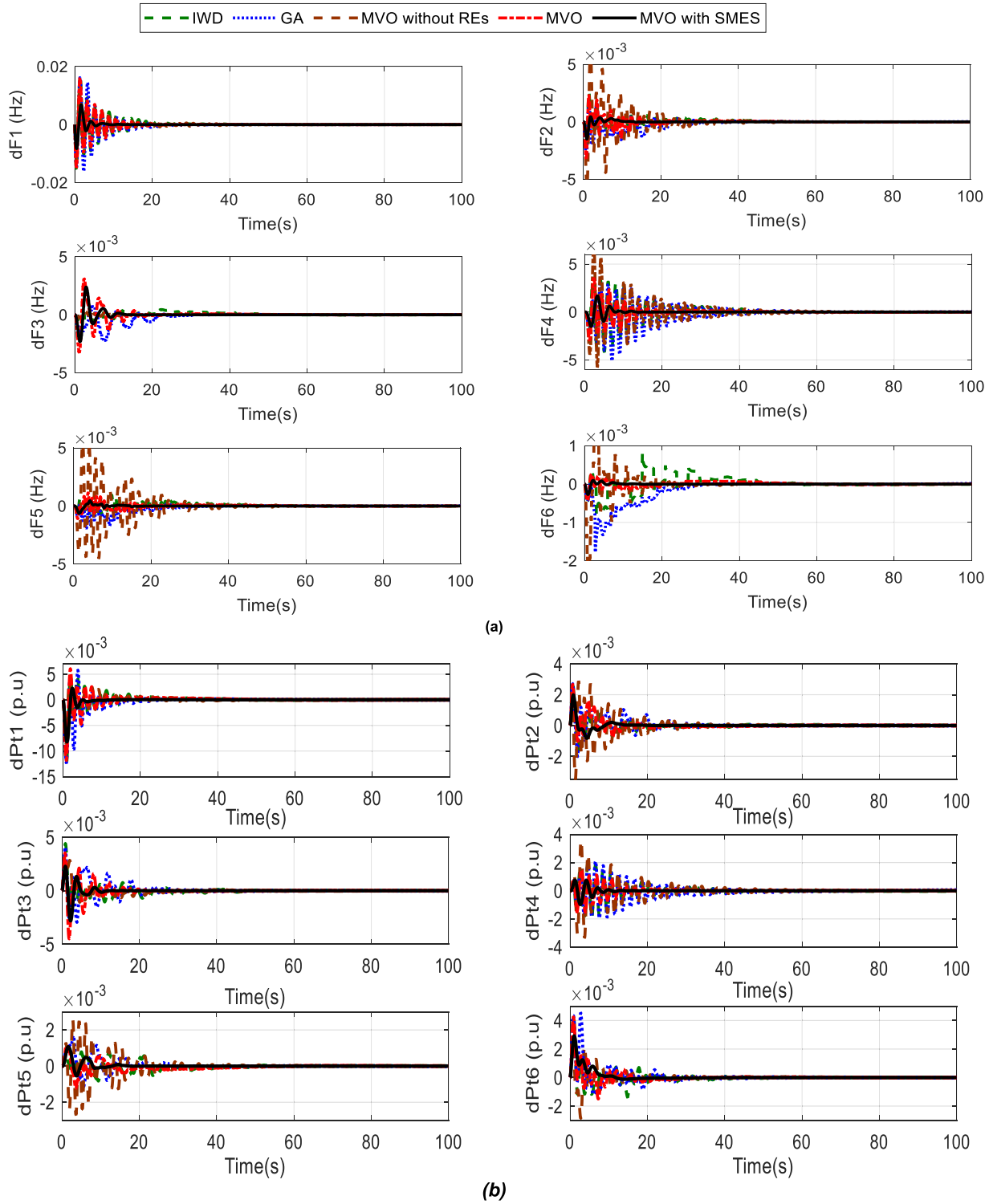

FIGURE 11. (a) Frequency aberration (dF_i), and (b) Tie-line power aberration ($dP_{tie,i}$) for 1% load disturbance applied on area 1.

r_4 are random numbers in the range of [0, 1], *TDR* is the rate of the traveling distance and WEP is the probability of the presence of wormholes. Exploration and local optima prevention are emphasized by high TDR and small WEP, which are improved using eqns. (13) and (14) respectively. Low TDR and high WEP enhance the exploitation process and provide an accurate assessment of the optimal global results. TDR and WEP can be expressed as follows:

$$TDR = 1 - \frac{Iter^{(1/p)}}{Iter_{max}^{(1/p)}} \tag{15}$$

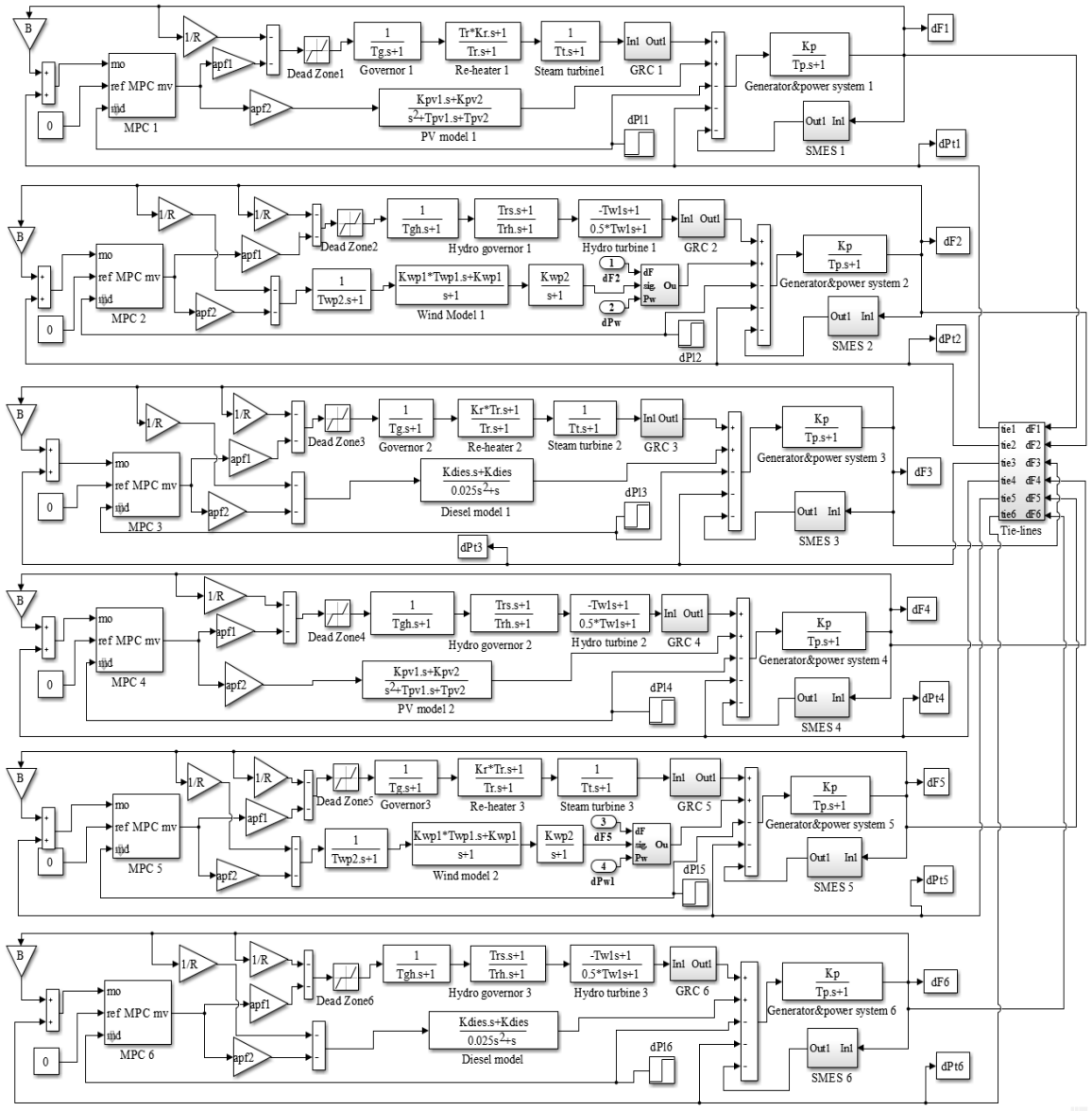

(a)

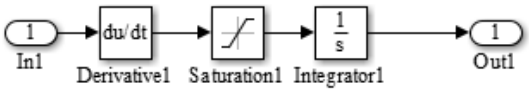

(b)

FIGURE 12. (a) GRC model (b) Simulink model of nonlinear six-interconnected system.

$$WEP = W_{min} + Iter \times \left(\frac{W_{max} - W_{min}}{Iter_{max}} \right) \qquad (16)$$

where $W_{\min}$, $W_{\max}$, *Iter,* $Iter_{\max}$, and p are minimum, maximum, current iteration, maximum number of iterations, and precision of exploitation over iterations respectively. The optimization process starts with initializing the collected random variables representing the universes. At each iteration, universe factors with elevated fitness migrate through black/white holes towards universes with small fitness scores. Meanwhile, through wormholes, each universe meets a random theoretical transition to the finest universe

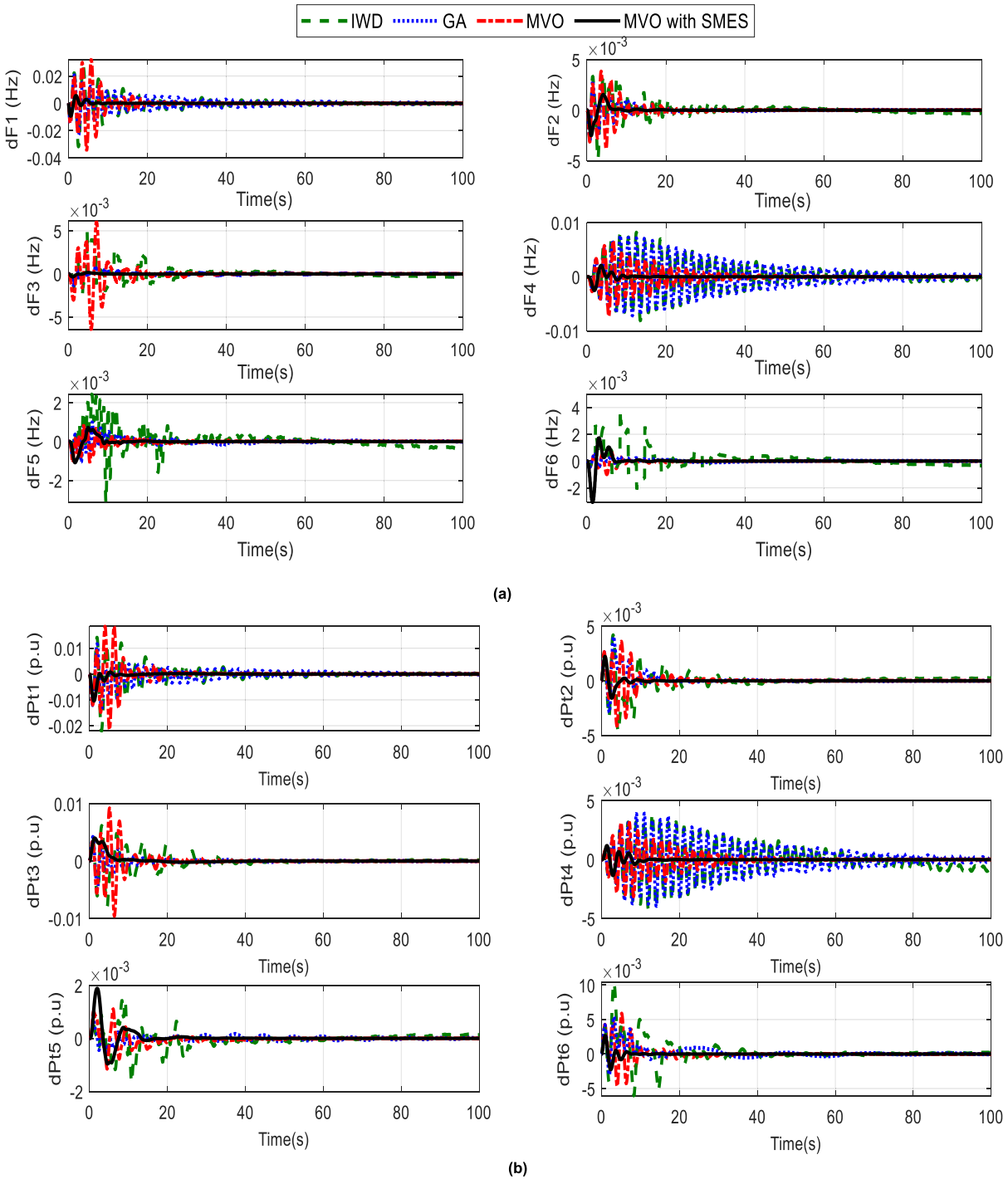

FIGURE 13. System time responses of dF_i and $dP_{tie,\,i}$ for nonlinear six-interconnected system.

in its variables. This process is repeated to a pre-defined peak amount of iterations. Furthermore, the MVO algorithm retains the finest alternative and uses it to affect the rest of the alternatives.

III. THE PROPOSED OPTIMIZATION PROBLEM

In this section, the theory of the model predictive control (MPC) is discussed. Additionally, the LFC with the proposed approach combined MVO and MPC is explained.

A. MODEL OF PREDICTIVE CONTROL

MPC is a recent approach based on predicting the future of the process to be controlled and widely used in industrial processes. The MPC is online optimization with various variables formulations and has the ability to treat the constraints. Fig. 5 shows the MPC approach theory, where the sample interval is the vertical axis. The main idea of MPC is to measure the difference between the reference signal and the current system output signal and then predict the output at

TABLE 3. Performance specifications of linear six-interconnected system for 1% load disturbance applied on area 1.

Signal	MPC-IWD with installed RESs			MPC-GA with installed RESs			MPC-MVO without RESs		
	Ts (s)	Us (Hz)	Ms (Hz)	Ts (s)	Us (Hz)	Ms (Hz)	Ts (s)	Us (Hz)	Ms (Hz)
dF1	24.3279	-0.0151	0.0168	25.7469	-0.0161	0.0163	37.6425	-0.0123	0.0116
dF2	45.4884	-0.0033	0.0026	39.3154	-0.0033	0.0018	40.6074	-0.0057	0.0063
dF3	88.0110	-0.0006	0.0005	30.4110	-0.0023	8.84-4	32.4553	-0.0003	0.0003
dF4	50.9722	-0.0042	0.0033	53.2311	-0.0051	0.0032	50.3884	-0.0057	0.0070
dF5	80.1472	-0.0010	0.0010	45.7645	-0.0019	1.60-4	45.4708	-0.0045	0.0057
dF6	80.2960	-0.0008	0.0008	39.3031	-0.0018	3.81e-4	27.46631	-0.0026	0.0031
dPtie1	33.9322	-0.0126	0.0048	22.3156	-0.0123	0.0057	38.0669	-0.0088	0.0040
dPtie2	41.6153	-0.0018	0.0027	43.3032	-0.0020	0.0027	41.7617	-0.0035	0.0029
dPtie3	45.8737	-0.0012	0.0044	41.4649	-0.0029	0.0041	41.0688	-0.0010	0.0032
dPtie4	50.4807	-0.0019	0.0020	--	-0.0020	0.0021	50.8215	-0.0033	0.0036
dPtie5	56.1273	-0.0008	0.0009	43.9473	-0.0011	0.0017	45.10755	-0.0027	0.0026
dPtie6	37.2951	-0.0014	0.0044	37.4282	-0.0012	0.0045	33.2747	-0.0028	0.0026
Signal	MPC-MVO with installed RESs			MPC–MVO with installed RESs and SMES		
	Ts (s)	Us (Hz)	Ms(Hz)	Ts (s)	Us (Hz)	Ms (Hz)
dF1	19.2465	-0.0147	0.0161	8.2758	-0.0083	0.0068
dF2	43.2732	-0.0032	0.0023	13.7697	-0.0015	0.0004
dF3	40.2826	-0.0033	0.0031	12.6600	-0.0023	0.0024
dF4	42.9058	-0.0029	0.0035	12.8775	-0.0015	0.0017
dF5	54.7284	-0.0011	0.0011	18.2065	-0.0006	0.0004
dF6	84.9491	-0.0004	0.0003	13.2802	-0.0003	0.0001
dPtie1	34.0514	-0.0118	0.0060	7.9600	-0.0082	0.0022
dPtie2	39.0600	-0.0010	0.0027	13.8713	-0.0008	0.0020
dPtie3	19.9416	-0.0045	0.0035	11.1492	-0.0028	0.0023
dPtie4	32.4644	-0.0015	0.0015	13.4399	-0.0010	0.0008
dPtie5	52.5040	-0.0012	0.0011	16.4860	-0.0005	0.0011
dPtie6	27.9921	-0.0015	0.0042	18.1214	-0.0001	0.0029

intervals of time until the output signal converges to the reference one [53], [54].

The structure of MPC is shown in Fig. 6, it comprises prediction and control units. The prediction unit is responsible for expecting the future performance of the system according to the current output. The objective function constraint is minimized by the control unit with the aid of the prediction unit output [55]. The aim of the optimization process is minimizing the difference between the predicted response and the reference one, as well as the control effort that is subjected to prescribed constraint [56]. The input and output of each area can be written as follows:

$$x_p(k+1) = A_p x_p(k) + BS_i u_p(k) \quad p = 1, 2, \ldots, n \tag{17}$$

$$y_p(k) = S_o^{-1} C x_p(k) + S_o^{-1} D S_i u_p(k) \quad p = 1, 2, \ldots, n \tag{18}$$

where A, B, C, and D are the state space matrices, S_i and S_o are diagonal matrices of input and output respectively, u_p is a vector of dimensionless plant input variables, and n is the number of the plants. In MPC, two phases are employed to calculate the current move (u_k) which are estimation and optimization phases. In the first one, the MPC movement is dependent on the system state which is represented by the current and future control variables ($\bar{y}_k, \bar{y}_{k+1}, \ldots, \bar{y}_{k+p}$).

In the optimization phase, target points, constraints, and disturbances are represented over a finite interval as $(k+1, k+2, \ldots, k+P)$ where P is a finite integer number. After that, MPC calculates the M movements of u_k, u_{k+1}, $\ldots$, u_{k+M-1}, where $1 \leq M \leq P$. The movement of MPC is determined via solving the following expression:

$$\underbrace{\min}_{u(k),\ldots,u(k+p-1)} \sum_{i=1}^{p} \left[Q\left(r_{k+1} - \hat{y}_{k+1}\right)^2 + R\left(\Delta u_{k+i-1}\right)^2 \right] \tag{19}$$

Subject to, $u_{min} \leq u_{k+1} \leq u_{max}$

$$y_{min} \leq \hat{y}_{k+1} \leq y_{max}$$

$$|\Delta u_{k+i}| \leq \Delta u_{max} \tag{20}$$

B. THE PROPOSED LFC WITH MPC

The proposed MPC used in this work is based on linear time-invariant (LTI) and constructed with the aid of the MPC toolbox in Matlab Simulink. LTI can be calculated by using MPC toolbox in Simulink, LTI for first area can be calculated by removing MPC from the other area and disconnecting the tie-line. However, LTI of the other areas can be computed in similar way. For nonlinear system, both governor dead zone and generation rate constrain are illuminated.

The proposed objective function can be written as follows:

The optimal parameters of the proposed MPC based LFC (T, P, M, R, and Q) are evaluated via the proposed methodology of MVO such that minimizing the ITAE of

TABLE 4. Sensitivity analysis for linear six-interconnected system for 1% load disturbance applied on area 1.

						T_g						
Signal		-50%			-25%			+25%			+50%	
	Ts(s)	Us(Hz)	Ms(Hz)	Ts(s)	Us(Hz)	Ms (Hz)	Ts(s)	Us(Hz)	Ms(Hz)	Ts(s)	Us(Hz)	Ms(Hz)
dF1	11.4008	-0.0083	0.0067	8.4501	-0.0083	0.0068	8.0433	-0.0083	0.0069	7.8510	-0.0083	0.0069
dF2	15.3355	-0.0015	0.0004	13.7662	-0.0015	0.0004	13.7777	-0.0015	0.0005	13.7929	-0.0015	0.0005
dF3	12.7067	-0.0023	0.0024	12.6849	-0.0023	0.0024	12.5780	-0.0023	0.0024	12.4296	-0.0023	0.0024
dF4	16.9405	-0.0015	0.0017	14.3682	-0.0015	0.0017	12.7413	-0.0015	0.0017	12.5953	-0.0015	0.0017
dF5	18.1806	-0.0006	0.0004	18.1928	-0.0006	0.0004	18.2223	-0.0006	0.0004	18.2406	-0.0006	0.0004
dF6	15.7972	-0.0003	9.46e-5	15.7667	-0.0003	9.53e-5	13.3210	-0.0003	9.73e-5	13.3401	-0.0003	9.84e-5
dPtie1	10.6911	-0.0082	0.0022	10.5078	-0.0082	0.0022	7.5216	-0.0082	0.0022	9.0456	-0.0083	0.0023
dPtie2	13.7905	-0.0008	0.0020	14.1183	-0.0008	0.0020	17.2794	-0.0008	0.0020	13.7460	-0.0008	0.0020
dPtie3	11.5604	-0.0028	0.0023	11.3198	-0.0028	0.0023	11.0567	-0.0028	0.0023	10.9983	-0.0028	0.0023
dPtie4	15.2908	-0.0010	0.0008	15.1164	-0.0010	0.0008	12.0451	-0.0010	0.0008	11.8964	-0.0010	0.0008
dPtie5	16.6226	-0.0006	0.0011	16.5515	-0.0005	0.0011	16.4245	-0.0005	0.0011	16.3672	-0.0005	0.0011
dPtie6	17.7695	-0.0001	0.0029	17.8652	-0.0001	0.0029	19.0110	-0.0001	0.0029	19.1553	-0.0001	0.0029
ITAE		**0.3392**			**0.3241**			**0.3187**			**0.3441**	
						T_r						
Signal		-50%			-25%			+25%			+50%	
	Ts(s)	Us(Hz)	Ms(Hz)	Ts(s)	Us(Hz)	Ms(Hz)	Ts(s)	Us(Hz)	Ms(Hz)	Ts(s)	Us(Hz)	Ms(Hz)
dF1	7.8165	-0.0083	0.0068	8.1058	-0.0083	0.0068	8.3613	-0.0083	0.0068	8.4111	-0.0083	0.0068
dF2	13.0826	-0.0015	0.0004	13.6868	-0.0015	0.0004	13.8031	-0.0015	0.0004	13.8216	-0.0015	0.0004
dF3	12.6834	-0.0023	0.0023	12.6620	-0.0023	0.0024	12.6643	-0.0023	0.0024	12.6664	-0.0023	0.0024
dF4	12.6023	-0.0015	0.0016	12.7961	-0.0015	0.0017	14.2310	-0.0015	0.0017	14.3499	-0.0015	0.0017
dF5	18.1572	-0.0006	0.0004	18.1813	-0.0006	0.0004	18.2252	-0.0006	0.0005	18.2385	-0.0006	0.0005
dF6	13.3389	-0.0003	0.0001	13.2973	-0.0003	0.0001	13.2854	-0.0003	0.0001	13.311	-0.0003	0.0001
dPtie1	9.3048	-0.0082	0.0021	8.4125	-0.0082	0.0022	7.8770	-0.0082	0.0022	7.8289	-0.0082	0.0023
dPtie2	19.5357	-0.0008	0.0020	13.9454	-0.0008	0.0020	13.8510	-0.0008	0.0020	13.8423	-0.0008	0.0020
dPtie3	10.9941	-0.0028	0.0023	11.0805	-0.0028	0.0023	11.2071	-0.0028	0.0023	11.2550	-0.0028	0.0023
dPtie4	11.8568	-0.0010	0.0008	12.0859	-0.0010	0.0008	14.8766	-0.0010	0.0008	15.0302	-0.0010	0.0008
dPtie5	16.2244	-0.0005	0.0011	16.3782	-0.0005	0.0011	16.5597	-0.0006	0.0011	16.6136	-0.0006	0.0011
dPtie6	30.4628	-0.0001	0.0029	24.5761	-0.0001	0.0029	17.8275	-0.0001	0.0029	17.8158	-0.0001	0.0029
ITAE		**0.4027**			**0.3398**			**0.3073**			**0.3131**	
						T_t						
Signal		-50%			-25%			+25%			+50%	
	Ts(s)	Us(Hz)	Ms(Hz)	Ts(s)	Us(Hz)	Ms(Hz)	Ts(s)	Us(Hz)	Ms(Hz)	Ts(s)	Us(Hz)	Ms(Hz)
dF1	13.8037	-0.0083	0.0065	11.4143	-0.0083	0.0067	7.8861	-0.0083	0.0070	12.3160	-0.0083	0.0071
dF2	15.6373	-0.0015	0.0004	15.3599	-0.0015	0.0004	13.8030	-0.0015	0.0005	13.8510	-0.0015	0.0005
dF3	16.7070	-0.0023	0.0024	12.7663	-0.0023	0.0024	12.3875	-0.0023	0.0024	12.1082	-0.0023	0.0024
dF4	17.2943	-0.0015	0.0017	16.9792	-0.0015	0.0017	12.6340	-0.0015	0.0017	12.4813	-0.0015	0.0017
dF5	18.1779	-0.0006	0.0005	18.1856	-0.0006	0.0005	18.2377	-0.0006	0.0004	18.2713	-0.0006	0.0004
dF6	18.6644	-0.0003	8.86e-5	18.3002	-0.0003	9.22e-5	13.3350	-0.0003	0.0001	13.3474	-0.0003	0.0001
dPtie1	10.8455	-0.0082	0.0020	10.7160	-0.0082	0.0021	8.9814	-0.0083	0.0023	9.2166	-0.0083	0.0024
dPtie2	13.7064	-0.0008	0.0020	13.7422	-0.0008	0.0020	17.0546	-0.0008	0.0020	17.4904	-0.0008	0.0020
dPtie3	15.9263	-0.0027	0.0023	11.6291	-0.0028	0.0023	11.0045	-0.0028	0.0023	10.9512	-0.0029	0.0023
dPtie4	20.6326	-0.0010	0.0008	15.3150	-0.0010	0.0008	11.9510	-0.0010	0.0008	21.9697	-0.0010	0.0008
dPtie5	16.7809	-0.0006	0.0010	16.6199	-0.0006	0.0010	16.3772	-0.0005	0.0010	16.2969	-0.0005	0.0010
dPtie6	17.7154	-0.0002	0.0029	17.7926	-0.0001	0.0029	19.0748	-0.0001	0.0029	21.3350	-0.0001	0.0029
ITAE		**0.3631**			**0.3365**			**0.3488**			**0.4674**	
						K_{pv1}						
Signal		-50%			-25%			+25%			+50%	
	Ts(s)	Us(Hz)	Ms(Hz)	Ts(s)	Us(Hz)	Ms(Hz)	Ts(s)	Us(Hz)	Ms(Hz)	Ts(s)	Us(Hz)	Ms(Hz)
dF1	8.1818	-0.0082	0.0068	8.2308	-0.0082	0.0068	8.31710	-0.0083	0.0069	8.3542	-0.0084	0.0069
dF2	13.7739	-0.0015	0.0004	13.7715	-0.0015	0.0004	13.7677	-0.0015	0.0004	13.7662	-0.0015	0.0004
dF3	12.5993	-0.0023	0.0024	12.6512	-0.0023	0.0024	12.6703	-0.0023	0.0024	12.6784	-0.0023	0.0024
dF4	12.8298	-0.0015	0.0017	12.8540	-0.0015	0.0017	12.8986	-0.0015	0.0017	14.1164	-0.0015	0.0017
dF5	18.2164	-0.0006	0.0004	18.2115	-0.0006	0.0004	18.2021	-0.0006	0.0005	18.1978	-0.0006	0.0005
dF6	13.2682	-0.0003	9.50e-5	13.2737	-0.0003	9.56e-5	13.287	-0.0003	9.70e-5	13.2954	-0.0003	9.77e-5
dPtie1	7.9203	-0.0081	0.0022	7.9439	-0.0082	0.0022	7.9718	-0.0083	0.0022	7.9811	-0.0083	0.0023
dPtie2	13.9478	-0.0008	0.0020	13.9031	-0.0008	0.0020	13.8445	-0.0008	0.0020	13.8230	-0.0008	0.0020
dPtie3	11.0951	-0.0028	0.0023	11.1211	-0.0028	0.0023	11.1806	-0.0028	0.0023	11.2137	-0.0028	0.0023
dPtie4	12.1434	-0.0010	0.0007	13.1495	-0.0010	0.0008	13.6085	-0.0010	0.0008	13.6963	-0.0010	0.0008
dPtie5	16.4603	-0.0005	0.0011	16.4736	-0.0005	0.0011	16.4979	-0.0006	0.0011	16.5088	-0.0006	0.0011
dPtie6	18.6046	-0.0001	0.0029	18.2625	-0.0001	0.0029	18.0454	-0.0001	0.0029	17.9874	-0.0001	0.0030
ITAE		**0.3086**			**0.3107**			**0.3174**			**0.3212**	

TABLE 5. Comparative analysis of errors for nonlinear six-interconnected system for 1% load disturbance applied on area 1.

Algorithm	ITAE	IAE	ITSE	ISE
IWD with installed RESs	24.2447	0.9868	0.0461	0.0047
GA with installed RESs	18.7711	0.7574	0.0375	0.0031
MVO with installed RESs	4.9068	0.5398	0.0243	0.0047
MVO with installed RESs and SMES	0.6054	0.1142	0.0005	0.0003

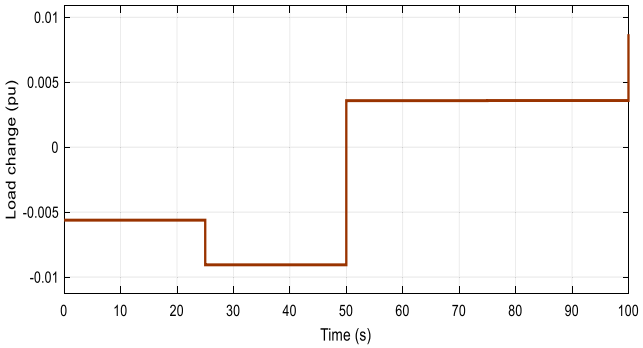

FIGURE 14. Variable load disturbance.

frequencies and tie-line power aberrations.

$$ITAE = \int_0^t \sum_{i=1}^{n} \left(|dF_i| + \left|dP_{tie,i}\right|\right) t.dt \tag{21}$$

where t is the simulation time, dF_i is the aberration of frequency in area i and $dP_{tie,i}$ is the power aberration in tie-line power in area i.

The proposed LFC with MPC optimized via MVO is shown in Fig. 7, while Fig. 8 presents the flowchart of the proposed MVO. The constraints of MPC parameters are selected as $0.1 \leq T \leq 10$, $10 \leq P \leq 10$, $1 \leq M \leq 10$, $1 \leq R \leq 10$ and $1 \leq Q \leq 10$ [30].

The pseudo code of MPC with LFC is presented as follows:

Algorithm 1 MPC Based LFC Optimized via MVO

1. Construct LTI or state-space model of the system with installed LFC.
2. Initialize MPC_i parameters *(T, P, M, R, Q)*
3. Convert the continuous system to discrete system with the aid of eqn. (17),
4. When start Sim model in Simulink, the MPC measures the disturbance (dP_L) and the output signal (dF_i).
5. Apply (u_{k+1}) to the system using eqn. (20) to predict the output.
6. *for* $i = 1:P$;
7. *If* $dF_i \neq$ *ref. signal.*
8. Next sample time $(k = k+i)$,
9. end
10. end

TABLE 6. Optimal parameters of MPC for nonlinear six-interconnected system for 1% load disturbance applied on area 1.

Algorithms	Controller	Parameter				
		T	P	M	R	Q
IWD with installed RESs	MPC1	1.6399	8.0000	4.0000	8.0423	7.4852
	MPC2	9.0632	9.0000	3.0000	7.3326	3.9996
	MPC3	1.1480	9.0000	4.0000	5.6043	9.1600
	MPC4	6.2519	8.0000	4.0000	8.2759	6.4167
	MPC5	2.2157	6.0000	4.0000	1.6197	5.9103
	MPC6	2.0846	10.000	4.0000	6.0360	5.8766
GA with installed RESs	MPC1	1.8410	8.0000	3.0000	3.8230	4.0340
	MPC2	2.120	4.0000	3.0000	6.6530	8.1050
	MPC3	0.9450	8.0000	4.0000	3.5360	5.5710
	MPC4	1.5920	6.0000	2.0000	2.9090	3.3490
	MPC5	0.6390	5.0000	4.0000	6.3520	4.3860
	MPC6	2.0500	5.0000	3.0000	9.5850	2.0160
MVO with installed RESs	MPC1	1.2957	9.0000	4.0000	9.6994	3.4623
	MPC2	8.5300	4.0000	4.0000	9.7626	1.0000
	MPC3	0.1000	9.0000	2.0000	4.4758	3.7529
	MPC4	1.3851	5.0000	2.0000	6.7006	6.8789
	MPC5	9.9819	6.0000	3.0000	9.2145	8.9296
	MPC6	3.1049	6.0000	4.0000	9.3418	1.8979
MVO with installed RESs and SMES	MPC1	5.2341	5.0000	2.0000	7.5193	9.4448
	MPC2	0.1000	7.0000	4.0000	1.0150	4.6160
	MPC3	7.9867	9.0000	1.0000	8.8033	1.2579
	MPC4	3.2126	5.0000	2.0000	5.1404	9.3077
	MPC5	4.1478	5.0000	4.0000	8.1528	7.9908
	MPC6	0.1019	5.0000	1.0000	6.4400	9.6855

TABLE 7. Performance analysis of nonlinear six-interconnected system.

Signal	MPC-IWD with installed RESs			MPC-GA with installed RESs			MPC-MVO with installed RESs			MPC–MVO with installed RESs and SMES		
	Ts (s)	Us (Hz)	Ms (Hz)	Ts (s)	Us (Hz)	Ms (Hz)	Ts (s)	Us (Hz)	Ms (Hz)	Ts (s)	Us (Hz)	Ms (Hz)
dF1	97.5487	-0.0317	0.0272	96.4417	-0.0230	0.0207	27.8034	-0.0343	0.0320	8.95487	-0.0094	0.0056
dF2	--	-0.0048	0.0035	52.5743	-0.0031	0.0029	34.5536	-0.0038	0.0038	13.4984	-0.0025	0.0015
dF3	--	-0.0023	0.0049	92.7098	-0.0019	8.09e-4	33.7375	-0.0064	0.0061	28.5832	-0.0003	0.0002
dF4	--	-0.0081	0.0082	--	-0.0072	0.0076	48.8385	-0.0073	0.0066	15.7678	-0.0025	0.0021
dF5	--	-0.0031	0.0024	95.5177	-0.0010	0.0010	52.6664	-0.0011	0.0008	25.9007	-0.0011	0.0007
dF6	--	-0.0021	0.0039	88.1897	-4.53e-4	5.70e-4	32.8961	-0.0010	0.0007	13.5770	-0.0031	0.0017
dPtie1	71.9238	-0.0220	0.0141	93.9093	-0.0142	0.0117	27.4704	-0.0216	0.0185	12.2278	-0.0104	0.0008
dPtie2	--	-0.0047	0.0042	39.6484	-0.0029	0.0041	31.8108	-0.0041	0.0036	12.6856	-0.0016	0.0022
dPtie3	95.6243	-0.0079	0.0062	69.1283	-0.0049	0.0042	33.0002	-0.0097	0.0092	33.3507	-0.0002	0.0040
dPtie4	--	-0.0042	0.0040	--	-0.0040	0.0039	52.5307	-0.0031	0.0032	17.2512	-0.0013	0.0012
dPtie5	--	-0.0017	0.0014	98.6141	-.5.20e-4	7.30e-4	50.3862	-0.0012	0.0011	25.4282	-0.0010	0.0019
dPtie6	62.6743	-0.0061	0.0104	89.8723	-0.0030	0.0054	36.1026	-0.0047	0.0059	12.8796	-0.0023	0.0027

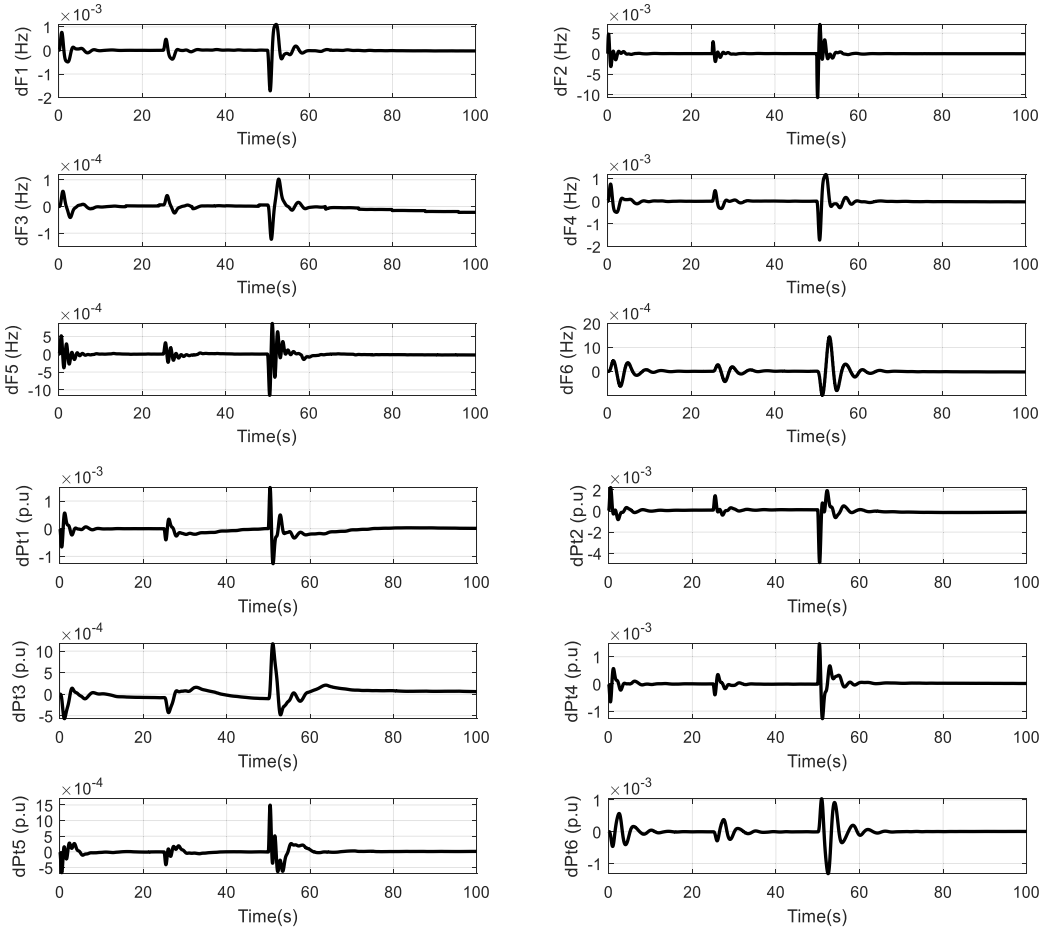

FIGURE 15. System time responses for variable load disturbance applied on area 2.

IV. SIMULATION RESULTS

The optimal parameters of the proposed MPC based LFC are determined using the proposed MVO with considering ITAE as objective function. The controlling parameters of MVO are 50 universes and 100 iterations. The system under study comprises six different plants including RESs. Additionally, the effects of the governor dead zone and generation rate constraint (GRC) of thermal plants are considered. The SMES capacity and parameters are taken from Ref. [49].

A. LINEAR MULTI-INTERCONNECTED SYSTEM

The constructed system composes six interconnected plants. The first area has thermal generating unit with PV, the second one is hydro plant coupled with WT. The third area is thermal

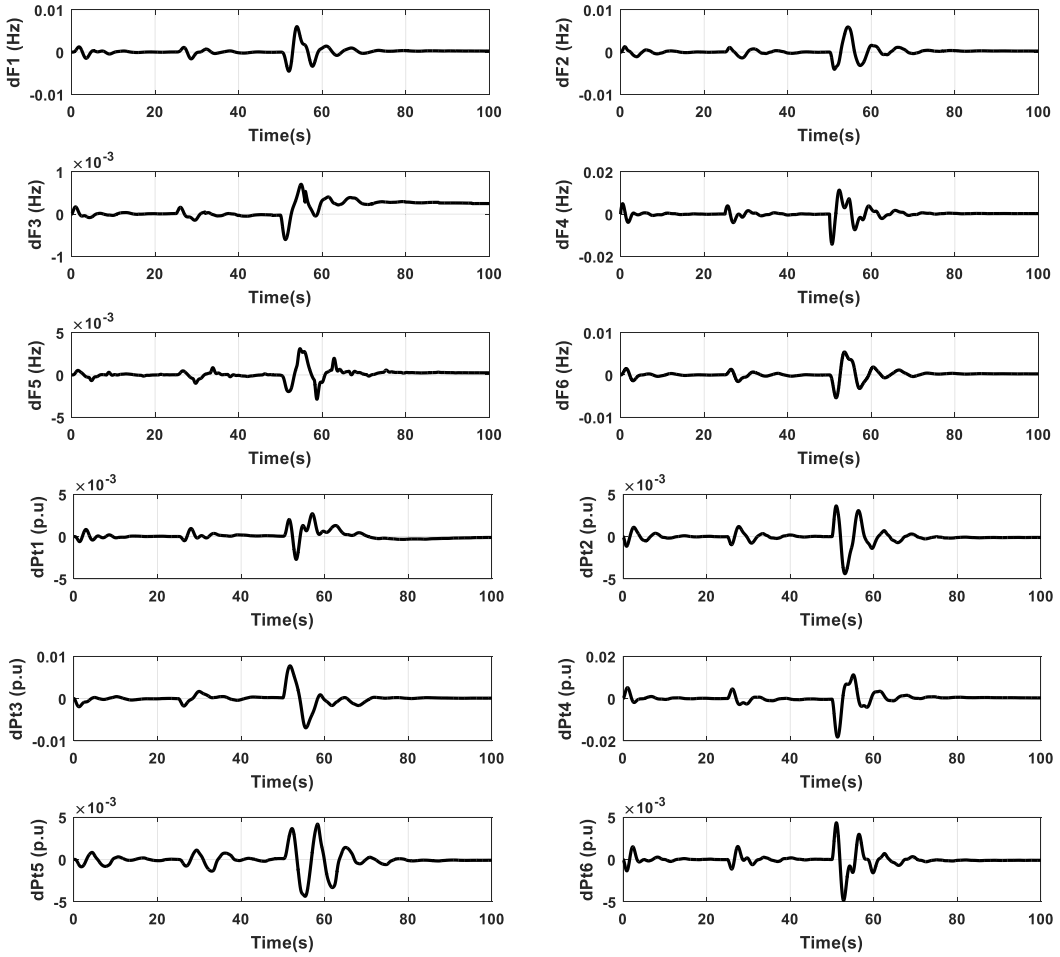

FIGURE 16. System time responses for variable load disturbance applied on area 4.

plant coupled with DG, the fourth area has a hydro generating unit with PV. The fifth area comprises thermal plant with WT, and the last one includes hydro unit and DG. It is assumed that, all plants have storage system of SMES. The Simulink model of the proposed multi-interconnected system is shown in Fig. 9. Regarding to the constructed system shown in Fig. 9, the block diagrams of PV and thermal plants are constructed based on the model given in Ref. [1] while the models hydro, wind turbine, and DG based plants given in Ref. [27], [44] are presented. The parameters of the constructed system are given in Table 8 in Appendix A. This architecture is proposed to study and implement the proposed LFC in large multi-interconnected system comprising RESs. The change in solar radiation for PV based plant and wind speed for WT based plant are modeled as step inputs that represent the load disturbance. This means the load disturbance occurs on PV or WT based plants represents the solar radiation and wind speed respectively. The first study case is performed by assuming a load disturbance of 1% applied on the first area. The obtained results via the proposed MVO are compared to those obtained via intelligent water drops algorithm (IWD) [57] and genetic algorithm (GA) for the constructed system with and without SMES. IWD is selected as comparative approach as It's a nature-inspired algorithm and population-based optimizer like MVO which depends on initializing probable solution using upper and lower bounds of variables of to be designed. Moreover, both approaches are similar in optimization process composing exploration and exploitation search phases. Furthermore, the availability of the proposed MVO based LFC is confirmed by selecting IWD that was not previously applied to design LFC. Fig. 10 shows the performance of the fitness function during implementing the optimizer for the constructed system with and without SMES. The obtained optimal error, integral time absolute error (ITAE), integral absolute error (IAE), integral time square error (ITSE), and integral square error (ISE)) are tabulated in Table 1. It's clear that, the MPC optimized via the proposed MVO succeeded in achieving the minimum error compared to the others. In case of missing the RESs, the designed LFC via the proposed MVO has a great effect on the obtained results. As it achieves ITAE of 3.2348 without RESs based plants. However, when the RESs based plants are considered the objective function becomes 0.3131. The optimal parameters of the proposed LFC are given in Table 2.

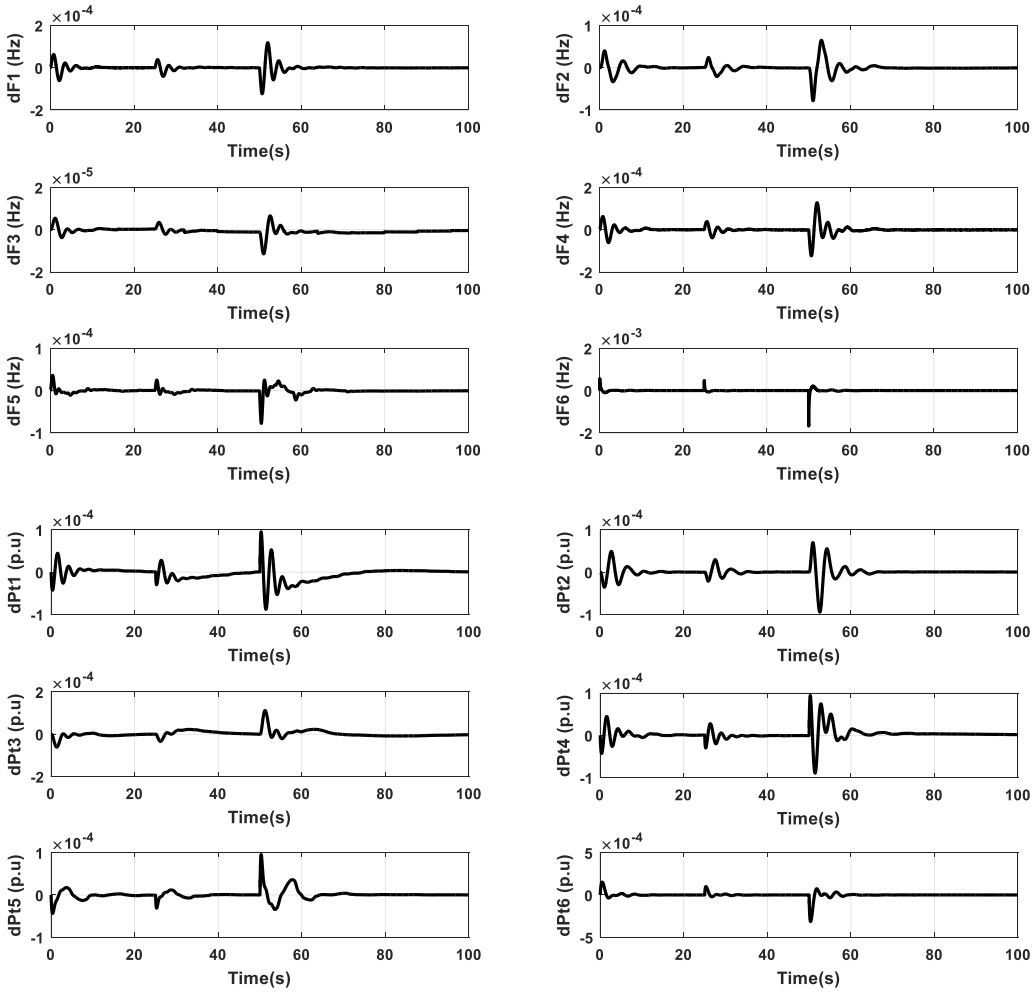

FIGURE 17. System time responses for variable load disturbance applied on area 6.

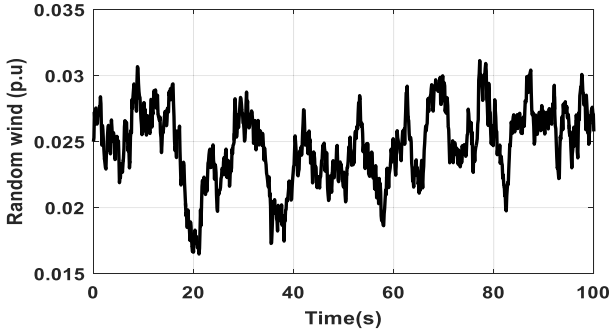

FIGURE 18. Random wind speed variation.

The results given in Fig. 11 and Table 3 are obtained via applying IWD and GA for the system with installed RESs. However, the obtained results via MVO are obtained for three cases which are system without installed RESs, system with installed RESs only, and system with installed RESs and SMES. The deviations in frequencies and tie-line powers are shown in Fig. 11. Additionally, settling time (Ts), undershoot (Us), and overshoot (Ms) of their time responses are calculated and compared to IWD and GA as given in Table 3. One can get that, the performances of the frequencies and tie-line power deviations obtained via the proposed MPC are the best compared to IWD and GA.

B. SENSITIVITY ANALYSIS

To confirm the validity and competence of the proposed LFC, it has been investigated under the variation of the system parameters. Sensitivity analysis is implemented on a linear six-interconnected system via changing some parameters of thermal and PV plants like T_g, T_r, T_t, and K_{pv1} in ranges of $\pm 25\%$ and $\pm 50\%$ with considering SMES. Table 4 tabulates the obtained results of the performance criteria and ITAE. It's confirmed that, the proposed optimal controller is robust to the variations of system parameters.

C. NONLINEAR MULTI-INTERCONNECTED SYSTEM

The proposed controller is incorporated in a nonlinear six-interconnected system considering the governor dead

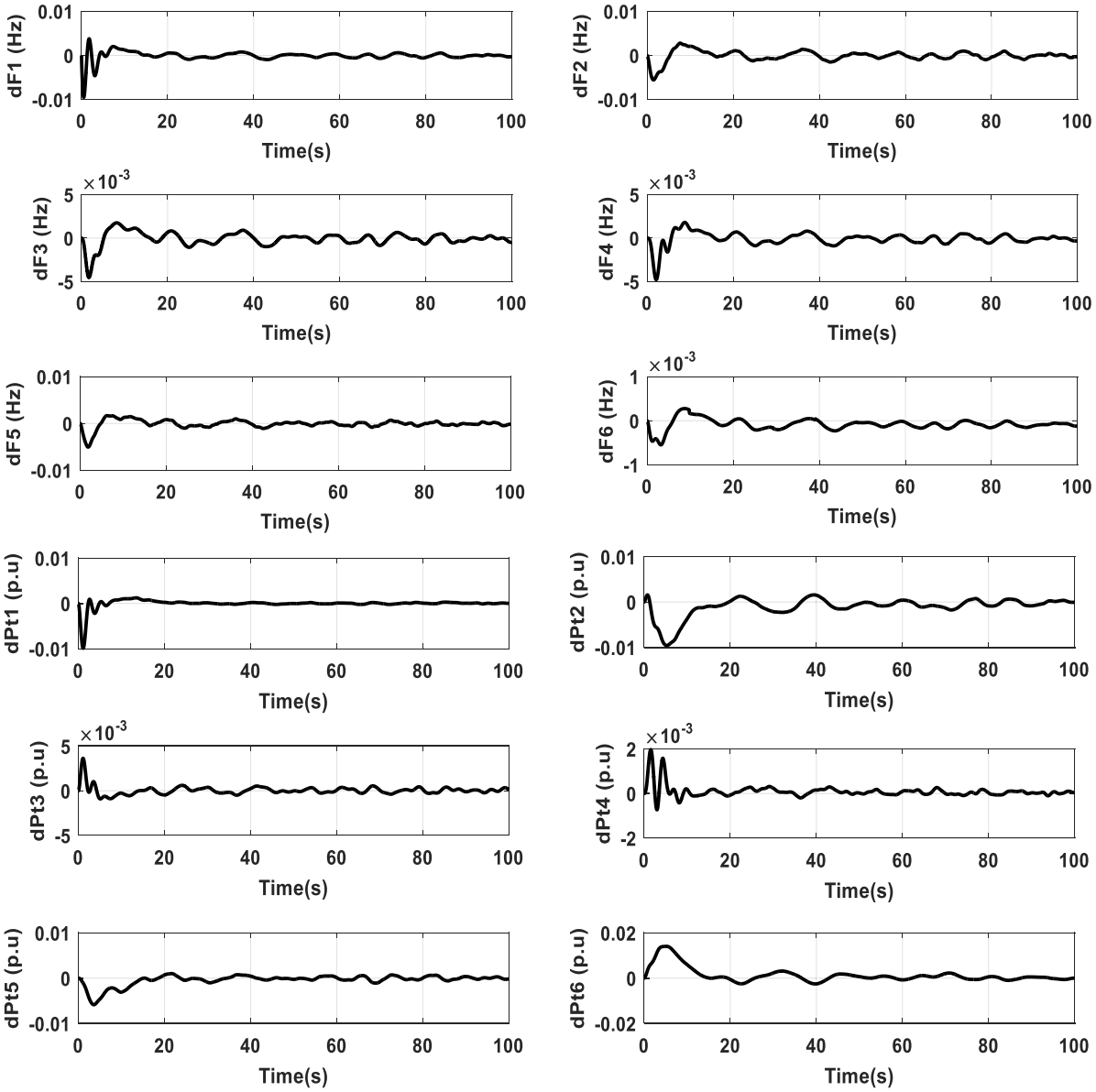

FIGURE 19. System time responses for variable wind speed and 1% load disturbance applied on area 1.

band (GDB) and generation rate constraint with considering SMES. Fig. 12 illustrates the Simulink model of the nonlinear six-interconnected system. Similar to the linear multi-interconnected system given in Fig. 9, the constructed system shown in Fig. 12 is constructed with the aid of models given in Refs. [3], [27]. A load disturbance of 1% is applied on area 1. Table 5 tabulates the values of ITAE, IAE, ITSE, and ISE obtained via the proposed approach in comparison with the others. However, the optimal parameters of the proposed MPC-LFC are given in Table 6 for all studied approaches. The best fitness function is 0.6054 obtained via the proposed MPC-LFC optimized via MVO with SMES. The time responses of the frequencies and tie-line powers aberrations are shown in Fig. 13. The performance specifications of the time responses obtained via MVO and the others are tabulated in Table 7. The results given in Fig.13 and Table 7 are obtained via applying IWD, GA, and MVO on the system with installed RESs. Moreover, the proposed MVO is applied for the system with installed RESs and SMES. The curves and data given in Table 7 confirmed the excellence of the proposed LFC for nonlinear six-interconnected system.

D. EFFECT OF VARIABLE LOAD DISTURBANCE

It's important to investigate the proposed MPC-LFC optimized via MVO in case of variable load disturbance. The presented disturbance is assumed to be in the range [−1%, 1%] applied on the second area as shown in Fig. 14. The aberrations in the frequencies and tie-line powers at variable

load disturbance are shown in Fig. 15. It's important confirm the stability of the constructed system with installed the proposed LFC, this is done via applying the variable load shown in Fig. 14 on the fourth and sixth areas. the aberrations in the frequencies and tie-line powers for A4 and A6 are shown in Figs. 16 and 17 respectively. The obtained responses confirmed the robustness of MPC to maintain stable system under variable load disturbance applied on different areas.

E. EFFECT OF VARIABLE WIND POWER

In order to confirm the competence of the proposed MPC-LFC optimized via MVO, the effect of variable wind power is analyzed on the proposed system given in Fig. 12. In this case, variable wind speed shown in Fig. 18 is applied on WT installed in area 2 and area 5 with considering 1% load disturbance applied on area 1. The aberrations in the frequencies and tie-line powers at such case are shown in Fig. 19.

The obtained time responses of the frequencies and tie-line powers obtained via the proposed MPC confirmed the validity and competence of the proposed LFC in achieving a reliable multi-interconnected system not only for the fixed disturbance but also under variable disturbance and variable wind power. The excessive analysis performed in this work and the obtained results represent a qualitative and quantitative support that confirms the validity and efficiency of the proposed optimized LFC based MPC in all studied cases.

V. CONCLUSION

A novel structure of load frequency control (LFC) incorporated in multi-interconnected system is proposed based on model predictive control (MPC) optimized via multi-verse optimizer (MVO). The integral time absolute error (ITAE) comprising the frequencies and tie-line powers deviations is proposed as objective function to be minimized. MVO is employed to calculate the optimal parameters of the proposed MPC. The constructed multi-interconnected system comprises reheat thermal, hydropower plants, PV system with MPPT, WT, and diesel generator (DG). The storage system of SMES is installed in all considered plants. Six different plants are interconnected and analyzed with different optimization approaches in two cases. The first one is a linear system, while the second on is a nonlinear system. Settling time, undershoot, and overshoot are calculated for the time responses of frequencies and tie-line powers aberrations obtained via MVO based LFC and compared to IWD and GA. IWD failed in obtaining acceptable results as it depends on large controlling parameter defined by the user which may cause falling in local optima. The proposed MVO based LFC with SMES achieved the preferable results due to less controlling parameters which avoid stuck in local optima. Moreover, MVO has powerful neighborhood exploration features. Furthermore, the usage of SMES assists in damping the frequency deviation as explained before. The system is investigated under varying some parameters with the proposed controller operated under variable load disturbance. The obtained results confirmed the superiority and the competence of the proposed MPC-LFC optimized via MVO in minimizing the frequencies and tie-line apowers deviations in case of operation under different load disturbances. Modifications in the exploration and exploitation processes followed in MVO are recommended in the future work to enhance the convergence rate of MVO.

APPENDIX

See Table 8 here.

TABLE 8. Parameters of six-interconnected system.

Parameter	Value	Parameter	Value
Thermal plant			
K_p	120 Hz/pu MW	T_t	0.3 sec
T_p	20 sec	T_r	10 sec
K_r	0.33 Hz/pu MW	T_g	0.08 sec
B	2.4 Hz/ pu MW	R	0.425 pu MW/Hz
Photovoltaic plant			
K_{pv1}	-18	T_{pv1}	100 s
K_{pv2}	900	T_{pv2}	50 s
Hydro			
T_{gh}	48.7 s	T_{rh}	10 s
T_{rs}	0.513 s	T_{W1}	1 s
Wind turbine plant			
K_{wp1}	1.25	T_{wp1}	6 s
K_{wp2}	1.4	T_{wp2}	0.041 s
Diesel generator plant			
K_{diesel}	16.5	apf1	0.65
apf2	0.35		
SMES			
T_1	0.2333 sec	T_4	0.2481 sec
T_2	0.016 sec	K_{smes}	0.2035
T_3	0.7087 sec	T_{smes}	0.03 sec

REFERENCES

[1] Y. Arya, "AGC of PV-thermal and hydro-thermal power systems using CES and a new multi-stage FPIDF-(1+PI) controller," *Renew. Energy*, vol. 134, pp. 796–806, Apr. 2019.
[2] A. Rahman, L. C. Saikia, and N. Sinha, "Automatic generation control of an interconnected two-area hybrid thermal system considering dish-stirling solar thermal and wind turbine system," *Renew. Energy*, vol. 105, pp. 41–54, May 2017.
[3] A. Fathy and A. M. Kassem, "Antlion optimizer-ANFIS load frequency control for multi-interconnected plants comprising photovoltaic and wind turbine," *ISA Trans.*, vol. 87, pp. 282–296, Apr. 2019.
[4] Y. Arya, "AGC of restructured multi-area multi-source hydrothermal power systems incorporating energy storage units via optimal fractional-order fuzzy PID controller," *Neural Comput. Appl.*, vol. 31, no. 3, pp. 851–872, Mar. 2019.
[5] P. Dash, L. C. Saikia, and N. Sinha, "Flower pollination algorithm optimized PI-PD cascade controller in automatic generation control of a multi-area power system," *Int. J. Electr. Power Energy Syst.*, vol. 82, pp. 19–28, Nov. 2016.
[6] B. P. Sahoo and S. Panda, "Improved grey wolf optimization technique for fuzzy aided PID controller design for power system frequency control," *Sustain. Energy, Grids Netw.*, vol. 16, pp. 278–299, Dec. 2018.

[7] M. Gheisarnejad, "An effective hybrid harmony search and cuckoo optimization algorithm based fuzzy PID controller for load frequency control," *Appl. Soft Comput.*, vol. 65, pp. 121–138, Apr. 2018.

[8] S. H. Shahalami and D. Farsi, "Analysis of load frequency control in a restructured multi-area power system with the Kalman filter and the LQR controller," *AEU Int. J. Electron. Commun.*, vol. 86, pp. 25–46, Mar. 2018.

[9] R. K. Sahu, S. Panda, and S. Padhan, "A novel hybrid gravitational search and pattern search algorithm for load frequency control of nonlinear power system," *Appl. Soft Comput.*, vol. 29, pp. 310–327, Apr. 2015.

[10] N. R. Babu and L. C. Saikia, "Automatic generation control of a solar thermal and dish-stirling solar thermal system integrated multi-area system incorporating accurate HVDC link model using crow search algorithm optimised FOPI minus FODF controller," *IET Renew. Power Gener.*, vol. 13, no. 12, pp. 2221–2231, Sep. 2019.

[11] R. K. Khadanga, A. Kumar, and S. Panda, "A novel modified whale optimization algorithm for load frequency controller design of a two-area power system composing of PV grid and thermal generator," *Neural Comput. Appl.*, vol. 32, no. 12, pp. 8205–8216, Jun. 2020, doi: 10.1007/s00521-019-04321-7.

[12] M. Sharma, R. K. Bansal, S. Prakash, and S. Asefi, "MVO algorithm based LFC design of a six-area hybrid diverse power system integrating IPFC and RFB," *IETE J. Res.*, pp. 1–14, Dec. 2018, doi: 10.1080/03772063.2018.1548908.

[13] W. Tasnin, L. C. Saikia, and M. Raju, "Deregulated AGC of multi-area system incorporating dish-stirling solar thermal and geothermal power plants using fractional order cascade controller," *Int. J. Electr. Power Energy Syst.*, vol. 101, pp. 60–74, Oct. 2018.

[14] A. Rahman, N. Sinha, and L. C. Saikia, "AGC of dish-stirling solar thermal integrated thermal system with biogeography based optimised three degree of freedom PID controller," *IET Renew. Power Gener.*, vol. 10, no. 8, pp. 1161–1170, Sep. 2016.

[15] Y. Arya, "Improvement in automatic generation control of two-area electric power systems via a new fuzzy aided optimal PIDN-FOI controller," *ISA Trans.*, vol. 80, pp. 475–490, Sep. 2018.

[16] M. Nandi, C. K. Shiva, and V. Mukherjee, "TCSC based automatic generation control of deregulated power system using quasi-oppositional harmony search algorithm," *Eng. Sci. Technol., Int. J.*, vol. 20, no. 4, pp. 1380–1395, Aug. 2017.

[17] A. H. G. Haroun and Y.-Y. Li, "Ant lion optimized fractional order fuzzy pre-compensated intelligent pid controller for frequency stabilization of interconnected multi-area power systems," *Appl. Syst. Innov.*, vol. 2, no. 2, p. 17, May 2019, doi: 10.3390/asi2020017.

[18] M. K. Sarkar, A. Dev, P. Asthana, and D. Narzary, "Chattering free robust adaptive integral higher order sliding mode control for load frequency problems in multi-area power systems," *IET Control Theory Appl.*, vol. 12, no. 9, pp. 1216–1227, Jun. 2018.

[19] M. Gheisarnejad and M. H. Khooban, "Design an optimal fuzzy fractional proportional integral derivative controller with derivative filter for load frequency control in power systems," *Trans. Inst. Meas. Control*, vol. 41, no. 9, pp. 2563–2581, Jun. 2019.

[20] Y. Sharma and L. C. Saikia, "Automatic generation control of a multi-area ST—Thermal power system using grey wolf optimizer algorithm based classical controllers," *Int. J. Electr. Power Energy Syst.*, vol. 73, pp. 853–862, Dec. 2015.

[21] R. Rajbongshi and L. C. Saikia, "Combined control of voltage and frequency of multi-area multisource system incorporating solar thermal power plant using LSA optimised classical controllers," *IET Gener., Transmiss. Distrib.*, vol. 11, no. 10, pp. 2489–2498, Jul. 2017.

[22] R. Mohammadikia and M. Aliasghary, "A fractional order fuzzy PID for load frequency control of four-area interconnected power system using biogeography-based optimization," *Int. Trans. Electr. Energy Syst.*, vol. 29, no. 2, pp. 1–17, Feb. 2019.

[23] S. Mishra, A. K. Barisal, and B. C. Babu, "Invasive weed optimization-based automatic generation control for multi-area power systems," *Int. J. Model. Simul.*, vol. 39, no. 3, pp. 190–202, Jul. 2019.

[24] S. M. Nosratabadi, M. Bornapour, and M. A. Gharaei, "Grasshopper optimization algorithm for optimal load frequency control considering predictive functional modified PID controller in restructured multi-resource multi-area power system with redox flow battery units," *Control Eng. Pract.*, vol. 89, pp. 204–227, Aug. 2019.

[25] M. Raju, L. C. Saikia, and N. Sinha, "Load frequency control of a multi-area system incorporating distributed generation resources, gate controlled series capacitor along with high-voltage direct current link using hybrid ALO-pattern search optimised fractional order controller," *IET Renew. Power Gener.*, vol. 13, no. 2, pp. 330–341, Feb. 2019.

[26] S. Dhundhara and Y. P. Verma, "Capacitive energy storage with optimized controller for frequency regulation in realistic multisource deregulated power system," *Energy*, vol. 147, pp. 1108–1128, Mar. 2018.

[27] R. K. Sahu, T. S. Gorripotu, and S. Panda, "A hybrid DE–PS algorithm for load frequency control under deregulated power system with UPFC and RFB," *AIN Shams Eng. J.*, vol. 6, no. 3, pp. 893–911, Sep. 2015.

[28] V. P. Singh, N. Kishor, and P. Samuel, "Improved load frequency control of power system using LMI based PID approach," *J. Franklin Inst.*, vol. 354, no. 15, pp. 6805–6830, Oct. 2017.

[29] A. Zamani, S. M. Barakati, and S. Yousofi-Darmian, "Design of a fractional order PID controller using GBMO algorithm for load–frequency control with governor saturation consideration," *ISA Trans.*, vol. 64, pp. 56–66, Sep. 2016.

[30] M. Elsisi, M. Soliman, M. A. S. Aboelela, and W. Mansour, "Optimal design of model predictive control with superconducting magnetic energy storage for load frequency control of nonlinear hydrothermal power system using bat inspired algorithm," *J. Energy Storage*, vol. 12, pp. 311–318, Aug. 2017.

[31] M. Elsisi, M. Soliman, M. A. S. Aboelela, and W. Mansour, "Improving the grid frequency by optimal design of model predictive control with energy storage devices," *Optim. Control Appl. Methods*, vol. 39, no. 1, pp. 263–280, Jan. 2018.

[32] H. M. Hasanien and A. A. El-Fergany, "Salp swarm algorithm-based optimal load frequency control of hybrid renewable power systems with communication delay and excitation cross-coupling effect," *Electr. Power Syst. Res.*, vol. 176, Nov. 2019, Art. no. 105938.

[33] E. Çelik, "Improved stochastic fractal search algorithm and modified cost function for automatic generation control of interconnected electric power systems," *Eng. Appl. Artif. Intell.*, vol. 88, Feb. 2020, Art. no. 103407.

[34] Y. A. Dahab, H. Abubakr, and T. H. Mohamed, "Adaptive load frequency control of power systems using electro-search optimization supported by the balloon effect," *IEEE Access*, vol. 8, pp. 7408–7422, Jan. 2020.

[35] P. C. Sahu, R. C. Prusty, and B. K. Sahoo, "Modified sine cosine algorithm-based fuzzy-aided PID controller for automatic generation control of multiarea power systems," *Soft Comput.*, pp. 1–18, Jan. 2020, doi: 10.1007/s00500-020-04716-y.

[36] D. Khamari, R. K. Sahu, T. S. Gorripotu, and S. Panda, "Automatic generation control of power system in deregulated environment using hybrid TLBO and pattern search technique," *AIN Shams Eng. J.*, pp. 1–21, Nov. 2019, doi: 10.1016/j.asej.2019.10.012.

[37] X. Shi, J. Hu, J. Yu, T. Yong, and J. Cao, "A novel load frequency control strategy based on model predictive control," in *Proc. IEEE Power Energy Soc. Gen. Meeting*, Jul. 2015, pp. 1–5.

[38] X. Shi, G. Wen, J. Cao, and X. Yu, "Model predictive power dispatch and control with price-elastic load in energy Internet," *IEEE Trans. Ind. Informat.*, vol. 15, no. 3, pp. 1775–1787, Mar. 2019.

[39] G. Wen, G. Hu, J. Hu, X. Shi, and G. Chen, "Frequency regulation of source-grid-load systems: A compound control strategy," *IEEE Trans. Ind. Informat.*, vol. 12, no. 1, pp. 69–78, Feb. 2016.

[40] M. Özdemir and D. Öztürk, "Comparative performance analysis of optimal PID parameters tuning based on the optics inspired optimization methods for automatic generation control," *Energies*, vol. 10, no. 12, p. 2134, Dec. 2017.

[41] P. Dahiya, P. Mukhija, A. R. Saxena, and Y. Arya, "Comparative performance investigation of optimal controller for AGC of electric power generating systems," *Automatika*, vol. 57, no. 4, pp. 902–921, Oct. 2016.

[42] S. M. Abd-Elazim and E. S. Ali, "Load frequency controller design of a two-area system composing of PV grid and thermal generator via firefly algorithm," *Neural Comput. Appl.*, vol. 30, no. 2, pp. 607–616, Jul. 2018.

[43] M. Tarkeshwar and V. Mukherjee, "A novel quasi-oppositional harmony search algorithm and fuzzy logic controller for frequency stabilization of an isolated hybrid power system," *Int. J. Electr. Power Energy Syst.*, vol. 66, pp. 247–261, Mar. 2015.

[44] C. S. A. Nandar, "Robust PI control of smart controllable load for frequency stabilization of microgrid power system," *Renew. Energy*, vol. 56, pp. 16–23, Aug. 2013.

[45] S. Ranjan, D. C. Das, S. Behera, and N. Sinha, "Parabolic trough solar–thermal–wind–diesel isolated hybrid power system: Active power/frequency control analysis," *IET Renew. Power Gener.*, vol. 12, no. 16, pp. 1893–1903, Dec. 2018.
[46] A. N. C. Supriyadi, H. Takano, J. Murata, T. Goda, and T. Hashiguchi, "Adaptive frequency control for hybrid wind-diesel power system using system estimator," in *Proc. IEEE Int. Conf. Power Syst. Technol. (POWERCON)*, Oct. 2012, pp. 1–6.
[47] J. Shi, Y. Xu, M. Liao, S. Guo, Y. Li, L. Ren, R. Su, S. Li, X. Zhou, and Y. Tang, "Integrated design method for superconducting magnetic energy storage considering the high frequency pulse width modulation pulse voltage on magnet," *Appl. Energy*, vol. 248, pp. 1–17, Aug. 2019.
[48] T. Watanabe and A. Ishiyama, "Superconducting magnetic energy storage system (SMES)," *J. Inst. Electr. Engineers Jpn.*, vol. 134, no. 8, pp. 546–548, 2014.
[49] A. Kumar and S. Suhag, "Effect of TCPS, SMES, and DFIG on load frequency control of a multi-area multi-source power system using multi-verse optimized fuzzy-PID controller with derivative filter," *J. Vib. Control*, vol. 24, no. 24, pp. 5922–5937, Dec. 2018.
[50] P. Bhatt, S. P. Ghoshal, and R. Roy, "Load frequency stabilization by coordinated control of thyristor controlled phase shifters and superconducting magnetic energy storage for three types of interconnected two-area power systems," *Int. J. Electr. Power Energy Syst.*, vol. 32, no. 10, pp. 1111–1124, Dec. 2010.
[51] M. Nandi, C. K. Shiva, and V. Mukherjee, "Frequency stabilization of multi-area multi-source interconnected power system using TCSC and SMES mechanism," *J. Energy Storage*, vol. 14, pp. 348–362, Dec. 2017.
[52] S. Mirjalili, S. M. Mirjalili, and A. Hatamlou, "Multi-verse optimizer: A nature-inspired algorithm for global optimization," *Neural Comput. Appl.*, vol. 27, no. 2, pp. 495–513, Feb. 2016.
[53] H. Bevrani, *Robust Power System Frequency Control* (Power Electronics and Power Systems), 2nd ed. New York, NY, USA: Springer, 2014.
[54] C. F. Eduardo, B. Carlos, E. F. Camacho, and C. B. Alba, *Model Predictive Control Advanced Textbooks in Control and Signal Processing*, 2nd ed. New York, NY, USA: Springer, 2007.
[55] M. Elsisi, M. Soliman, M. A. S. Aboelela, and W. Mansour, "Model predictive control of plug-in hybrid electric vehicles for frequency regulation in a smart grid," *IET Gener., Transmiss. Distrib.*, vol. 11, no. 16, pp. 3974–3983, Nov. 2017.
[56] T. H. Mohamed, H. Bevrani, A. A. Hassan, and T. Hiyama, "Decentralized model predictive based load frequency control in an interconnected power system," *Energy Convers. Manage.*, vol. 52, no. 2, pp. 1208–1214, Feb. 2011.
[57] H. S. Hosseini, "Intelligent water drops algorithm: A new optimization method for solving the multiple knapsack problem," *Int. J. Intell. Comput. Cybern.*, vol. 1, no. 2, pp. 193–212, Jun. 2008.

HOSSAM HASSAN ALI received the B.Sc. and M.Sc. degrees from the Electrical Department, Sohag University, Egypt, in 2012 and 2017, respectively. He is currently pursuing the Ph.D. degree. Since August 2017, he has been working as an Assistant Lecturer with the Electric Department, Faculty of Industrial Education, Sohag University. His research interests include renewable energy optimization, LFC, and optimal control and optimization techniques.

AHMED M. KASSEM received the B.Sc. degree in electrical engineering from Assiut University, Egypt, in 1991, the M.Sc. degree in electrical engineering from Eindhoven Technical University, The Netherlands, in 1999, and the Ph.D. degree in electrical engineering from Minia University, Minia, Egypt, in 2006. He has been the Dean of the Faculty of Engineering, Sohag University, Egypt, since 2014. He is currently a Professor of electrical engineering with the Electrical Department, Faculty of Engineering, Sohag University. He is an editorial board member for many journals and a consultant with the many industrial companies and a peer reviewer in many transactions, periodicals, and conferences. He has supervised many Ph.D. and M.Sc. thesis and has published more than 70 research articles. His research interests include smart energy grid, renewable energy management and control, energy storage, power electronics, power systems operation and control, renewable energy, electric drives and their control, electric vehicles and storage energy development, and intelligent control applications. He has got the Sohag University superiority award in 2018 in engineering sciences.

MUJAHED AL-DHAIFALLAH (Member, IEEE) received the B.Sc. and M.Sc. degrees in systems engineering from the King Fahd University of Petroleum and Minerals, Dhahran, Saudi Arabia, and the Ph.D. degree in electrical and computer engineering from the University of Calgary, Calgary, AB, Canada. He has been an Assistant Professor of systems engineering with the King Fahd University of Petroleum and Minerals, since 2009. His current research interests include nonlinear systems identification, control systems, optimization, artificial intelligence, and renewable energy.

AHMED FATHY received the B.Sc. (Hons.), M.Sc., and Ph.D. degrees in electrical engineering from Zagazig University, Egypt, in 2006, 2009, and 2014, respectively. Since January 2014, he has been working as an Assistant Professor with the Electric Power and Machines Department, Zagazig University. In February 2019, he has the scientific title of an Associate Professor with degree of scientific excellence. He has been an Assistant Professor with the Electrical Engineering Department, Faculty of Engineering, Jouf University, Saudi Arabia, since September 2015. He has been awarded many prizes for distinct research and for international publishing from Zagazig University and Jouf University. He has authored or coauthored more than 45 refereed journal articles and conference papers in his research interests, which include renewable energy optimization, optimal location of DGs in distribution networks, LFC, design of maximum power point trackers, applications of AI, and optimization techniques.